UNIVERSITY OF CALIFORNIA

Los Angeles

Theoretical Study of Electron Transfer in Organic Solar Cells

A dissertation submitted in partial satisfaction

of the requirements for the degree

Doctor of Philosophy in Chemistry

By

Randa Reslan

2015

ABSTRACT OF THE DISSERTATION

Theoretical Study of Electron Transfer in Organic Solar Cells

By

Randa Reslan

Doctor of Philosophy in Chemistry

University of California, Los Angeles, 2015

Professor Daniel Neuhauser, Chair

Organic solar devices can provide a cheaper alternative to the current silicon-based solar cell devices. The main disadvantage of organic photovoltaic is their low efficiency. Therefore there is a great need to better understand the mechanism of electron transfer in order to improve the efficiency of these devices. The main goal in my dissertation is to find a more accurate measure of electron transfer in these devices. I have been using theoretical methods to study electron transfer in fullerene derivatives, a common component of organic solar devices.

One such method that we have investigated is time-dependent split (TD-Split) to study A to B electron transfer by a TD evaluation of the lowest energy transition from the ground state

of the combined $(AB)^-$ system.

Another method that we have developed is the time-dependent ZINDO method (TD-ZINDO) to study absorption. ZINDO is a useful theoretical tool for systems of interest due to its capacity to handle large systems within reasonable times. We were able to perform explicit time calculations with a minimal basis set. The results were then compared with higher order DFT and TDDFT results.

We also used a DFT based method to calculate the charge transfer between very large solvated organic dimers like fullerenes from isolated dimer calculations. In this method, a delocalized bias is applied directly to the Fock matrix of the dimer until the extra electron is balanced between the two molecules in the dimers. Then the transfer rate can be calculated using Marcus theory. These theoretical methods differ in accuracy and speed. In my dissertation, I will present these different methods and compare them to each other and to experimental values.

This dissertation of Randa Reslan is approved.

William M. Gelbart

Henry Huang

Daniel Neuhauser, Committee Chair

University of California, Los Angeles

2015

TABLE OF CONTENTS

LIST OF FIGURES

LIST OF TABLES

ACKNOWLEDGMENTS

I would like to express the deepest appreciation to my committee chair, Daniel Neuhauser, who continually supported my research and study. Without his guidance and persistent help my research and dissertation would not have been possible. This work cannot be done without the effort and co-opetation from former and current group members, Lizette Bartelle, Michael Wall, Kenneth Lopata, Robert Boutelle, Yi Gao, Chen-Hsu Huang, Christopher Arntsen and Samuel Hernadez. I would like to express my gratitude to my family specially my husband, Badri, for his constant support. I would like to thank my daughters; Kristen and Jessica, my siblings, Nancy, Khaldoun and Reem, my Godparents; Rima and Vrej Azadian and all my friends for the constant support and encouragement. Last but not least, I would like to thank my parents Naim and Nour for raising me untraditionally, installing in me the love of knowledge and believing in my dreams.

Chapter 1

Chapter 1 is a version of: C. Arntsen, R. Reslan, S. Hernandez, Y. Gao, and D. Neuhauser, Direct delocalization for calculating electron transfer in fullerenes, International Journal of Quantum Chemistry 113, 1885 (2013). We are thankful to the DOE for support.

Chapter 2

Chapter 2 is a version of: L. Bartell, R. Reslan, M. Wall, R. Kennedy and D. Neuhauser, Electron transfer with TD-Split, a linear response time-dependent method. We are grateful to the DOE-EFRC program

Chapter 3

Chapter 3 is a version of: R. Reslan, K. Lopata, C. Arntsen, N. Govind, and D. Neuhauser, Electron transfer Beyond the static picture: A TDDFT/TD-ZINDO study of a pentacene dimer, The Journal of Chemical Physics 137, (2012). We are thankful to the DOE.

Chapter 4

Chapter 4 is a version of: K. Lopata, R. Reslan, M. Kowalska, D. Neuhauser, and K. Lowalski, Excited-state studies of polyacenes: A comparative picture using EOMCCSD, CR-EOMCCSD(T), range-separated (LR/RT)-TDDFT, TD-PM3, and TD-ZINDO, Journal of Chemical Theory and Computation, 7, 3686-3693 (2011). We are grateful to DOE-EFRC for support.

VITA

2001	B.S., Chemistry University of California, Los Angeles
2001	IGERT Fellowship
2008-present	Teaching Assistant Department of Chemistry and Biochemistry University of California, Los Angeles
2013	M.S., Chemistry University of California, Los Angeles

PUBLICATIONS

K. Lopata, R. Reslan, M. Kowalska, D. Neuhauser, N. Govind, and K. Kowalski. "Excited-state studies of polyacenes: A comparative picture using EOMCCSD, CR-EOMCCSD(T), range-separated (LR/RT)-TDDFT, TD-PM3 and TD-ZINDO", Journal of Chemical Theory and Computation, 7, 3686-3693 (2011)

L. Bartell, R. Reslan, M. Wall, R. Kennedy, D. Neuhauser, Electron transfer with TD-Split, a linear response time-dependent method, Chem. Phys. 391 (2011)

R. Reslan, K. Lopata, C. Arntsen, N. Govind, and D. Neuhauser, Electron transfer beyond the static picture: A TDDFT/TD-ZINDO study of a pentacene dimer. J. Chem. Phys. 137, 22A502 (2012)

C. Arnsten, R. Reslan, S. Hernandez, Y. Gao, and D. Neuhauser, Direct Delocalization for Calculating Electron Transfer in Fullerenes. International Journal of Quantum Chemistry 113, 1885-1889 (2013)

INTRODUCTION

There are many environmental, political, and financial reasons for the use of more renewable energy sources. Solar energy in particular is available, environmentally friendly, sustainable and abundant. Photovoltaics (PV) are the instruments that convert solar energy into direct current electricity using semiconducting materials. Inorganic photovoltaics (IPV), made from inorganic semiconductors such as silicon, have been studied since the 1950s and used in application since the 1960s. On the other hand, organic photovoltaics (OPV) are based on organic materials which consist mainly of a polymer donor and a fullerene acceptor. The most common electron acceptors in organic photovoltaic devices are fullerene derivatives, specifically [6,6]-phenyl-C_{61}-butyric acid methyl ester (PCBM)(see Figure 0.1). OPV devices have been getting much attention lately since they are inexpensive alternatives to IPV. The efficiency of these devices has been increased in the last few year but it is still around 10%, almost three times less than that of the best IPVs [1-2].

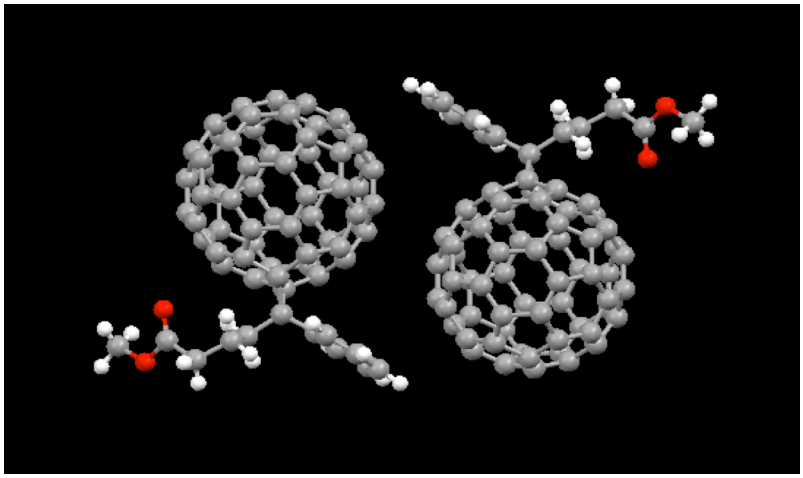

Figure 0.1: PCBM is most common electron acceptors in organic photovoltaic devices

There is, therefore a great need to improve the efficiency of organic solar cells, and theory can be a useful tool in advancing that efficiency. One major obstacle to such improvement is our general lack of understanding of the mechanism of electron transfer processes in

fullerene derivatives. Such understanding is clearly needed in order to improve the efficiency of these devices.

The main mechanism of OPV can be summarized as the following. Upon irradiation with light, a photon is absorbed by the polymer producing an "exciton". The exciton is then separated into a hole and an electron. In other words, an electron is excited from the highest occupied molecular orbital (HOMO) to the lowest unoccupied molecular orbital (LUMO). Then the electron is transferred to the fullerene leaving a hole in the polymer. Then the hole and the electron are migrated to their respective opposite electrodes and thereby generate electric current (see Figure 0.2).

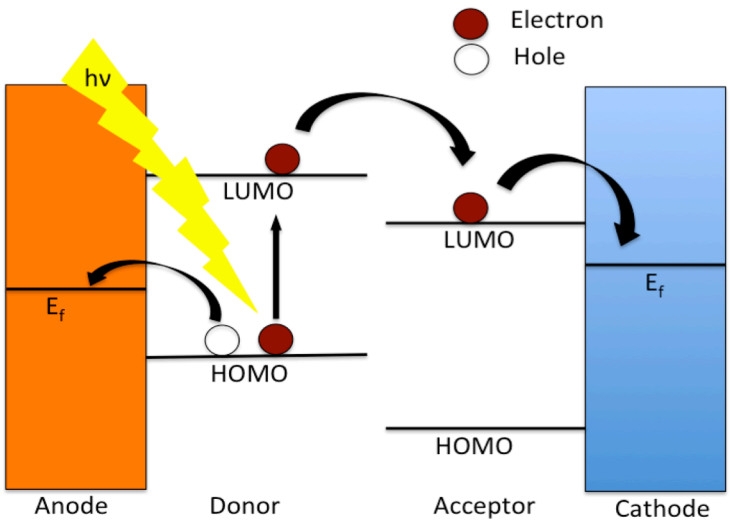

Figure 0.2: Schematic Diagram of electron transfer process in OPV. A photon will excite an electron in the donor. The electron will transfer to the acceptor leaving a hole. Both the electron and the hole will travel to the electrodes generating current.

There are many factors limiting the efficiency of an organic solar cell; such as insufficient photo-absorption, low electron and hole motilities, mismatch of energy levels between donor and acceptor,

and unwanted exciton recombination just to name a few [3]. Theory could, therefore be a tool to help us understand why some materials yield to more efficient devices than others and could be a predictive tool to screen materials prior to their use in actual devices.

The main goal in the present body of work is to find a more accurate measure of electron transfer in OPV devices. Since OPVs are systems of large size, there is a need to improve the computational description of OPV. Static simulations have the power to study the excited states in large systems but at the expense of accuracy. For example, semi-empirical quantum methods can study thousands of atoms and more. However, a better way to study excited states is using time dependent methods which are more accurate but computationally expensive and unfeasible for large systems.

In this dissertation, a variety of methods that we developed and used to study fullerenes are presented. The methods discussed all have advantages and disadvantages, so our main purpose will be to find a proper balance between accuracy and speed.

The time dependent semi-empirical methods and the other methods we use come from basic quantum mechanics. The electronic property of a molecule can be calculated by solving the Schrodinger equation,

$$H\psi = E\psi,$$

where H is the Hamiltonian operator for N electrons and M nuclei, which can be expressed as:

$$H = -\sum_{i=1}^{N}\frac{1}{2}\nabla_i^2 - \sum_{i=1}^{N}\frac{1}{2M_A}\nabla_A^2 - \sum_{i=1}^{N}\sum_{A=1}^{M}\frac{Z_A}{r_{iA}} + \sum_{i=1}^{N}\sum_{j>1}^{N}\frac{1}{r_{ij}} + \sum_{A=1}^{M}\sum_{B>A}^{M}\frac{Z_A Z_B}{R_{AB}}.$$

Here, electrons are represented by i and j and nuclei are represented by A and B; r repsents the distance and Z the atomic charge. The first term of H is the kinetic energy of the electrons and the second term the kinetics energy of the nuclei. The third term calculates the Coulomb attraction between the nuclei and electrons. The fourth term represents the repulsion between the electrons and the fifth the repulsion between the nuclei.

The Schrodinger equation can be solved exactly for hydrogen and other single electron system. As the systems get bigger, the solutions for the Hamiltonian rapidly become more complicated. Many numerical techniques can be used to solve the Hamiltonian where each has its advantages and disadvantages for specific systems.

Some of the earliest methods which attempt to solve the Schrodinger equation are methods which produce high accurate results[4]. They are manageable on small molecules. As the system gets bigger, the computations become very expensive. Hartee-Fock (HF) is an old and very common used ab initio method where a single-determinant approximation is used[4,5]. However ab initio methods are inefficient and expensive in treating large system even if the HF approximation is used making it limited to smaller system.

As a result, other quantum mechanical methods were developed to improve the efficiency and manage bigger systems. The most commonly used one is Density Functional Theory (DFT)[6]. As the name denotes it, DFT uses functional to express the Schrodinger equation as a function of charge density. Originally, the Schrodinger equation is expressed as function of position of all electrons (N), therefore it is a function with 3N arguments since each electron has x, y, and z coordinates. DFT will turn the Schrodinger equation into a function of change density, just a function of a single 3 dimensional coordinate, x, y, and z. DFT approximates the correlation and

exchange terms of the Hamiltonian into functionals to reduce the problem into a single density. The use of exchange and correlation functionals will result of a faster and more efficient DFT in comparison to ab initio methods. As the same time, DFT could be less accurate. The accuracy of DFT will also depend on the size of the basis sets that are used. The bigger basis sets will give more accurate results but are more computationally costly. Therefore DFT is accurate and efficient for small molecules but it will become very expensive for large molecules. Using smaller basis sets will result more efficient calculation, which handle bigger systems, but are less accurate.

An approach that can handle large molecules is semi-empirical methods such as PM3 and ZINDO. In semi-empirical methods, some pieces of information (such as two-electron integrals) are approximated or omitted. Therefore this method uses parameters that are obtained from direct measurements or by fitting the calculation to experimental results to correct this loss of information. The results of this method are fitted to experimental data or ab initio results. Since fitting the interactions is done using a minimal basis set, the parameterizations are more accurate than ab initio methods with small basis sets. In semi empirical methods, electron-electron interactions are considered but the matrix elements are parameterized. Semi-empirical methods use the frozen core approximation where the nuclei with the inner-shell electrons are treated as one unit. The frozen core interactions are calculated once. Therefore the electron-electron calculations are simplified since they will only include the valence electrons. These methods can handle large molecules very efficiently and can be more accurate than ab initio methods with smaller basis sets.

The semi-empirical methods that are mostly used throughout this dissertation are Parametric Model 3 (PM3) and Zerner's Intermediate Neglect of Differential Overlap(ZINDO). These methods like

any other semi-empirical method are very fast, can be used on large molecules and can be accurate when used on molecules that are similar to the molecules used in parameterization.

PM3 method uses the Modified Neglect of Diatomic Orbitals method (MNDO). In this method, the exchange and Coulomb integrals are considered between two different centers and the integrals between three or four centers are omitted. Therefore, parameters were developed to account for the absence of these integrals. The total molecular electronic energy, E is calculated as

$$E = \frac{1}{2}\sum_{\mu}\sum_{\nu} P_{\mu\nu}(H_{\mu\nu} + F_{\mu\nu}).$$

P is the density function, H is the core Hamiltonian matrix, and F is the Fock matrix. The core Hamiltonian is expressed as H_{ij}. The following equation represents terms in the diagonal of the Fock matrix since the electron in the same orbital in the same atom A.

$$H_{\mu\mu} = U_{\mu\mu} + \sum_{B} V_{\mu\mu\, B}$$

Here, U is the kinetic energy of the electron and $V_{\mu\mu}$ represents the attraction between an electron in atom A and the core of atom B. Simply, $H_{\mu\upsilon}$ the interactions between electrons in the same atom but on different orbitals with the core of the other atom B, is:

$$H_{\mu\upsilon} = \sum_{B} V_{\mu\nu\, B}\ .$$

Finally, $H_{\mu\lambda}$ describes the interaction between electron in different atoms A and B.

$$H_{\mu\lambda} = \frac{1}{2}(\beta^{A}_{\phi_\mu} + \beta^{B}_{\phi_\lambda})S_{\mu\lambda},$$

where β is the specific parameter that is associated each orbital, ϕ and S is the overlap matrix. Initially the density matrix. P is approximated as equal to the overlap matrix, S; then the Fock matrix is solved. The density matrix is then updated using the eighenvectors of the Fock marix. This

process is repeated until the electronic energy is converged or a tolerance level of density matrix variation is reached.

ZINDO is an improvement of INDO to cover wider range of elements, which was developed by Zerner and others. In ZINDO, only the valence electrons are treated, which is done via semi-empirical one-body (i.e., nuclear and core) parameters h_{ij} and two-body interaction parameters v_{ijkl}, which are fit to experimental data,

$$F_{ij} = h_{ij} + \sum_{kl} v_{ijkl} P_{ij},$$

P is the density matrix in the atomic orbital basis. Unlike Hartee-Fock and DFT, the interaction parameters are restricted to at most two-center.

Time Dependent-Density Functional Theory, TD-DFT, is an improvement of DFT that is much more accurate for excitation states[4-5,7]. It combines DFT with the time-dependent Schrodinger equation. The increase of accuracy of TD-DFT is the result of including polarization. As a result, TD-DFT is very expensive and becomes more costly as the size of the system increases. To increase the efficiency and accuracy, a linear response approach can be used with an efficient time evolution of TD-DFT. First the ground state of the system is determined then a pulse-like perturbation is applied. The system is finally evolved in time and a Fourier transform will produce the excitation energies. This method is accurate and efficient for small to medium sized molecules. As the size of the system is increased, this method becomes very expensive. Similarly, linear response can be combined with semi-empirical method like ZINDO to make TD-ZINDO. Initially, the ground state of the system is calculated then a pulse-like electric field is applied. The density matrix is evolve in time yielding of a dipole moment and a Fourier transform of the dipole moment will give

the excitation energies. The time-dependent response is computed using explicit time propagation via the von Neumann equation,

$$i\frac{\partial P'}{\partial t} = \left[F'\left(P'(t)\right), P'(t)\right].$$

The prime notation means matrices in the orthogonal molecular orbital (MO) basis. The actual propagation was carried out using a linear-response von Neumann operator

$$LZ \equiv \frac{dZ}{dt} = -i\frac{[F'(P_0' + \eta Z), P_0' + \eta Z] - [F'(P_0'), P_0']}{\eta},$$

where $Z(t) \equiv P'(t) - P_0'$ is the deviation of the MO density matrix from the initial state, and η is small parameter ensuring linearity. $Z(t)$ is propagated from the dipole perturbed ground state $Z_0 = -i[D, P_0']$ via a Chebyshev expansion[8-9], and the Fourier transform of the resulting time-dependent dipole moment yields the absorption spectrum, and thus the vertical excitation energies.

In the remaining parts of the introduction, I will introduce and summarize the body of the thesis, i.e., the papers published.

In the manuscript "Direct Delocalization for Calculating Electron Transfer in Fullerenes", the charge transfer between very large solvated fullerenes is calculated using isolated dimer calculations. This method mimics the bulk chemical environments in OPV films using solvation and electric field application.

Typically Marcus theory is used to calculate the electron transfer rate in symmetric organic solar cells

$$k_{MT} = \frac{2\pi}{\hbar}\left|H_{ij}\right|^2 (4\pi\lambda\kappa_B)^{-\frac{1}{2}} \exp\left(\frac{\left(\Delta E_{ij} + \lambda\right)^2}{4\lambda\kappa_B T}\right), \qquad H_{ij} = \langle\psi_i|H|\psi_j\rangle,$$

where k_{MT} is the electron transfer rate, H_{ij} is the transfer rate integral, λ is the reorganization energy, ΔE_{ij} is energy difference between the initial state "i" and the final state "j". The challenge is in defining the wave functions of the initial and the final state. This expression is appropriate when the electronic states within both the acceptor and donor are well isolated. However for large molecules like fullerenes, the distance between electronic states in the valence band is small, below 0.1eV. As a result, there is a need to sum over all initial excited states each with its own rearrangement energies due to the different coupling to the environment vibrational states. In addition, for larger molecules one uses a single particle approximation instead of calculating the true electronic states.

As a result, we use a modified Marcus formalism in calculating the total electron transfer rate as a sum over all the initial states:

$$k'_{MT} = \frac{2\pi}{\hbar}\sum_{ij} f(\epsilon_i - \mu_L)\left|H_{ij}\right|^2 (4\pi\lambda\kappa_B)^{-\frac{1}{2}} \exp\left(\frac{\left(\Delta E_{ij}+\lambda\right)^2}{4\lambda\kappa_B T}\right).$$

The Fermi Dirac occupation of the donor states is defined as

$$f(\epsilon_i - \mu_0) = \frac{1}{1+e^{\beta(\epsilon_i-\mu_0)}},$$

where ϵ_i is defined as the energy of the donor state. The transfer time is the inverse of the transfer rate, defined as :

$$\tau = \frac{1}{k'_{MT}}.$$

Here, we calculate the transfer rates for a range of values instead of calculating over all the possible values due to the high computational cost.

In calculating the transfer rate, the charge distribution for neutral combination AB is approximated as not perturbed by adding an extra electron. The difference in energy between LUMO and LUMO+1 for the neutral combination AB is then equal to the Marcus coupling term for identical dimers with delocalized orbitals. But the Marcus coupling term H_{AB} is in reality modified due to presence of an extra electron which should not be ignored. Also, the LUMO and LUMO+1 might be localized on one molecule so splitting might be high but not due to transition. In that case, a dimer calculation showes little transfer. Therefore there is a need to restore symmetry to overcome the different-environment problem in isolating dimer calculations.

Each monomer in noncentrosymmetric dimers experience different chemical environments, therefore dimers do not necessarily represent the bulk-like molecules. The order of the frontier orbital; LUMO and LUMO+1, involved in the electron transfer could be misplaced. For example, in isolated dimer calculation, where no delocalization potential is applied, both LUMO and LUMO+1 could be located on one molecule. Therefore, a dimer calculation may show little transfer between the molecules.

As a result, there is a need to correct the environment of isolated dimer to take into account the bulk-like environment. To correct that, we delocalize the LUMO and LUMO+1 across two molecules using two different methods.

The first method involves "solvating" the dimer with surrounding molecules. Since the system is large, it is computationally expensive to solvate explicitly large molecules. An alternative is to solvate the dimer with point charges. The values of the point charges are set self-consistently to equal the Mulliken charges on the atoms of the dimer. It is still difficult and costly to use point charges. In a simpler method labeled by us as the "Delocalizing Field" method, we apply an electric

field to the system with a value chosen to delocalize the frontier orbitals. This requires sweeping across a wide range of electric fields until the delocalization is achieved. Due to the large cost of DFT simulations on large systems, this method is still computationally expensive since it requires large number of DFT calculations.

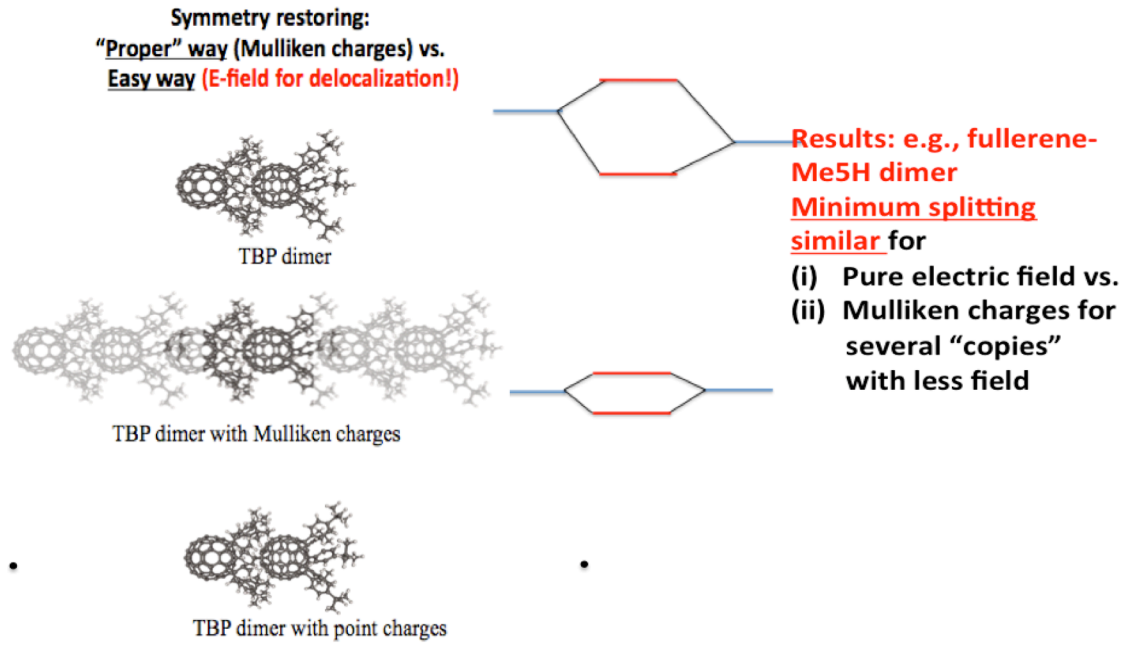

Figure 0.3 shows the environment of isolated dimer does not take into account the bulk-like environment. To correct that, we delocalize the LUMO and LUMO+1 across the two molecules using two different methods; Solvating with Mulliken charges on the atoms of the neighboring dimers. It is still difficult and costly to use point charges. A simpler method is the Delocalizing Field method.

Chapter I will present an even more efficient method, where we just perform single DFT calculation on a dimer system, then apply a bias directly to the post-self-consistent field (SCF) Fock matix until the extra electron is balanced between the two molecules. Then we calculate the transfer rate using Marcus theory. This method produces similar results and identical trends to the more complicated methods we try.

The manuscript entitled, "Electron transfer with TD-Split, a linear response time-dependent method" presents a simple method, time-dependent split (TD-Split) for $A \rightarrow B$ electron transfer by a TD evaluation of the lowest excitation energy form the ground state of the combined $(AB)^-$ system. As an example, the electron transfer between substituted fullerenes, primarily PCBM, was studied. Fullerenes are of great potential in organic solar cells. Although a lot of experimental progress has been made in the production of solar cells, any further improvement of efficiency is important for making them commercially successful.

Theoretical calculations could improve the development of solar cells, since electron transport is not yet clearly understood. It is not clear exactly what properties of organic molecules facilitate electron transport. An immediate solution is to synthesize various fullerenes with different ligands and test their transport. Many experimentalists are currently synthesizing these molecules. The disadvantage of this method is that it is costly and slow. Progress in this manner has not produced many candidates for commercial use beyond the initial fullerene-PCBM systems of Wudl et al but it is important to supplement this combinatorial by theoretical support.

In the search of new suitable molecules for organic solar cell, TD-PM3 can be modified to calculate the electron transport between molecules. As a result, this could help in determining the potential use of molecules prior to experimentally synthesizing them.

Another simple method for electron transfer that doesn't require time dependent technique is to apply a voltage or a bias in order to hold an electron in one of the molecule. The bias then relaxed and the change in charge distribution over both molecules is examined over time. The movement of the extra electron will be observed to determine the electron transfer. The drawback of this method is that the release of this bias will creates a lot of energy that push the electron to the other

molecules resulting in erratic, rather than regular results. As a result, it is difficult to quantify the rate.

TD-Split is similar to the previous method but makes use of time-dependent calculations resulting in more accurate results. This method is done using TD-PM3 to study bigger system with less time. This method can be done using TD-DFT as we will see in the next manuscript.

TD-Split is a linear response formula of the generic form

$$\delta A(t) = \langle \Psi(t) | A | \Psi(t) \rangle,$$

where is A is a perturbation operation and $|\Psi(t)\rangle$ is the perturbed ground state of the complete system including the extra electron delocalized over the donor and acceptor. This formula has an inherent advantage in that it has a very well defined initial state and any time-dependent dynamics is directly related to the transport.

In TD-Split, the initial state is the ground static density matrix associated with the whole (donor + acceptor) charged system. A time-dependent excitation is then applied and the response to this excitation peaks at a frequency relates to the transfer rate, its amplitude. This approach is inherently a linear response method, so the very efficient numerical tools developed for linear response in time-dependent approaches are immediately useable.

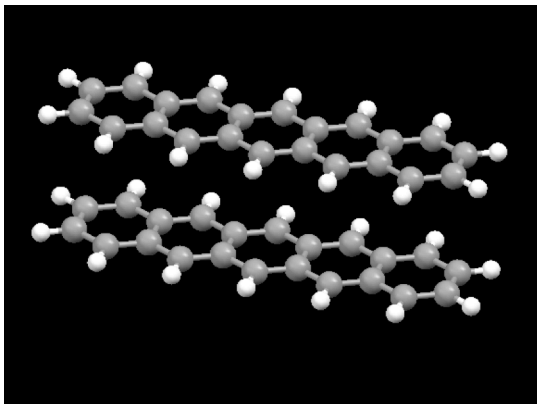

Figure 0.4: Pentacene dimer

Chapter III discusses transfer probabilities using different functionals and exact methods. Specifically as

mentioned there is a great need to calculate electron transfer rates and probabilities to understand many devices and processes. For example, in fullerene-based organic photovoltaic (OPVs), after photo-excitation of the light harvesting polymer, a charge-separated electron is first transferred to a nearby fullerene molecule, then subsequently shuttled to the electrode via a series of "hops" from one fullerene to another adjacent one. The success of an OPV often depends entirely on how readily electrons can be shunted form polymer to electrode without recombination with a hole. In general, this depends on the morphology of the device and the electron transfer probability between two fullerene molecules. The electron transfer in these systems is a complicated process involving the coupling between electronic, nuclear motion and the environment. Therefore it is difficult to calculate the transfer probabilities. Electron transfer calculations on model systems and simple analogues is a starting point that will leads us to understand the process in more complicated system and even to a real system. A lot of progress is attained in studying the electron transfer between isolated molecules. The electron transfer reaction $A^{-}B^{-} \rightarrow AB^{-}$ can be calculated using Marcus theory (see the reference) where the electronic coupling between the donor and the acceptor is assumed to be weak (non-adiabatic regime). Therefore the inter-conversion between the donor and acceptor adiabatic

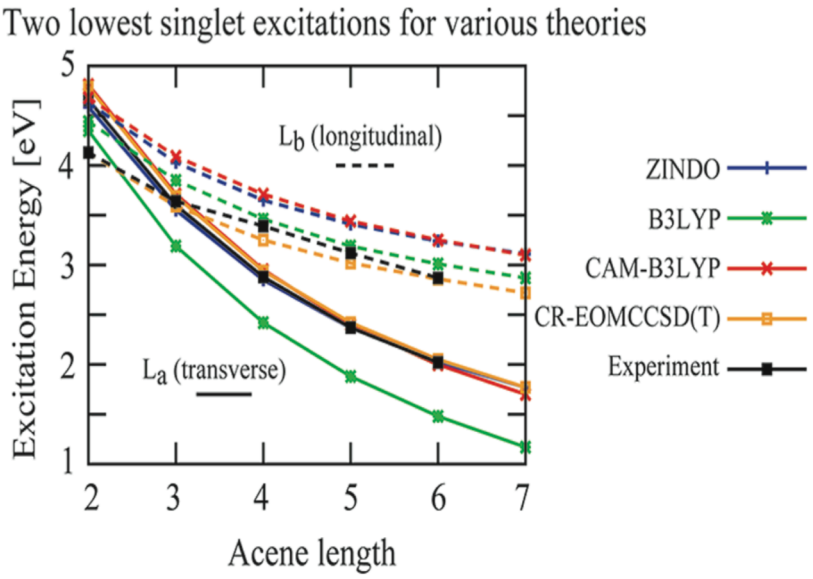

Figure 0.5: TD-ZINDO compared to more sophisticated TDDFT

potential energy surface can be calculated semi-classically. Although many theoretical approaches can be used within Marcus framework, density functional theory (DFT) has been mostly used, due its reasonable computational cost and its good accuracy. The main challenge in DFT is defining the initial and the final states in the transfer integral J in the Marcus formalism

$$J = |\langle \psi_F | H | \psi_I \rangle$$

In the following manuscript entitled, "Electron transfer beyond the static picture: A TDDFT/TD-ZINDO study of a pentacene dimer", TDDFT and TD-ZINDO used to study transfer of an extra electron between a pair of pentacene molecules. A measure of the electronic transfer integral is computed in a dynamic picture via the vertical excitation energy from a delocalized anionic ground state. With increasing dimer separation, this dynamical measurement of charge transfer is shown significantly larger than the commonly used static approximation (i.e., LUMO+1-LUMO of the neutral dimer, or HOMO-LUMO of the charged dimer), up to an order of magnitude higher at 6 Angstroms. Therefore static approximation for large separation will drastically underestimate transfer probability. These results offer a word of caution for calculations

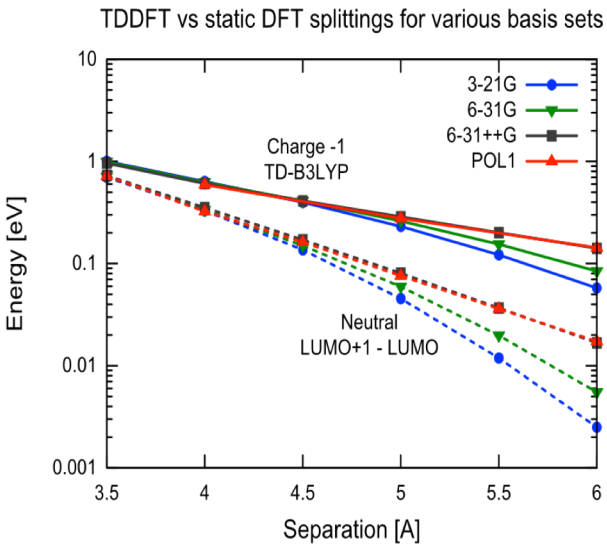

Figure 0.6: Static B3LYP splitting (dashed) and TD-B3LYP energies (solid) for a range of basis sets. Larger separation require a basis set with diffuse functions (e.g., 6-31++G and POL1) to avoid non-physical super-exponential falloff.

involving large separations, as in organic photovoltaics, where care must be taken when using static picture to model charge transfer.

Chapter III presents a study of electron transfer in pentacene dimers by presenting several methods for calculating the electron transfer integral, including time dependent density functional (TDDFT), a time-dependent semi-empirical method (TD-ZINDO), and time-independent methods using both neutral and anionic systems. Static calculations underestimate the transfer integral in comparison to time-dependent methods. TD-ZINDO underestimates the transfer integral, but a scaling factor can be applied to reproduce TDDFT results. Therefore, TD-ZINDO shows the same fall-off behavior as TDDFT at a fraction of cost.

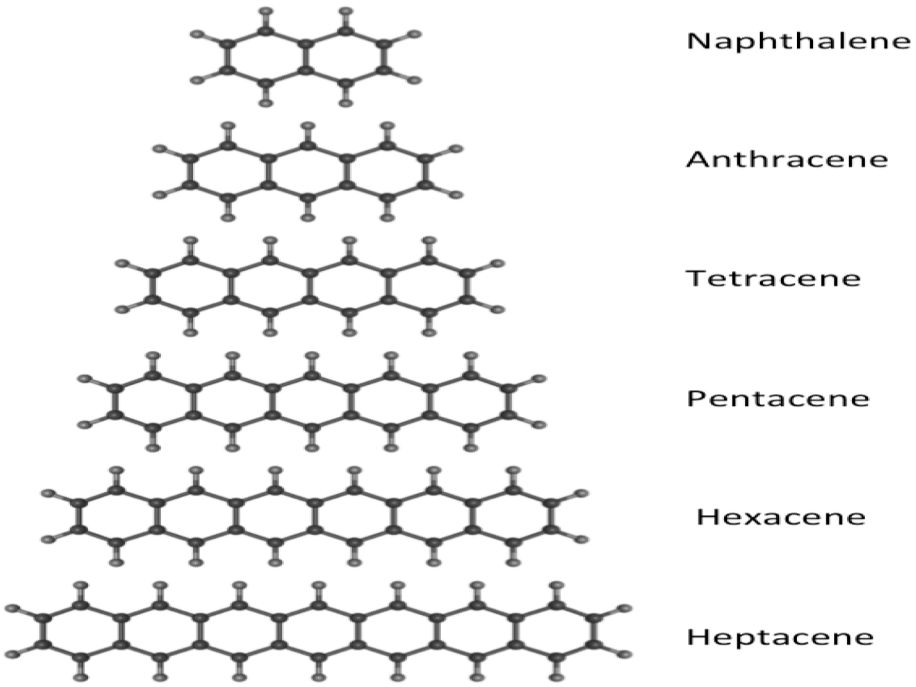

Figure 0.7: Structure of the acenes

In summary, chapter III introduces a time-dependent semi-empirical method. This method allows the treatment of very large molecules with reasonable efficiency and accuracy. The time-dependent

method was implemented with the semi-empirical method Zerner's Intermediate Neglect of Differential Overlap, ZINDO, so it is labeled TD-ZINDO. The TD-ZINDO method is applicable to spectra and also can be developed to study electron transfer between molecules.

In the manuscriped entitled "Excited-state studies of polyacenes: A comparative picture using EOMCCSD, CR-EOMCCSD(T), range-separated (LR/RT)-TDDFT, TD-PM3, and TD-ZINDO", the low-lying excited states (L_a and L_b) of polyacenes from naphthalene to heptacene are studied using different time-dependent computational methods.

Polyacenes consist of linearly fused benzene rings therefore they are rough prototypes for more complicated light harvesting system and act as fundamentally building blocks for many electronic devices. Therefore, careful analysis of the excitation of these molecules serves as a crucial test for accuracy and predictive power of a theoretical technique. These compounds have been studied extensively over last several years for many applications such as light-emitting diodes and photovoltaic cells, to name a few. The electronic properties of these materials are dictated by the π electrons that occupy the highest occupied and lowest occupied states. In a single molecule, the lowest valence excitations have $\pi - \pi^*$ character, and the two lowest valence excitations are commonly represented as the L_a (B_{2u} symmetry) and L_b (B_{3u} symmetry) states, respectively. The L_b represents the polarization along the long axis and it is the lowest excited state in naphthalene. The L_a represents the polarization along the short axis and it is the lowest state for acenes larger than anthracene. Both states L_a and L_b are almost the same for anthracene.

There have been many methods describing these excitations theoretically where DFT is the predominant method. This chapter details a systematic analysis based on high-level excited-state calculations using equation of motion coupled cluster with singles and doubles (EOMCCSD) and

completely renormalized equation of motion coupled cluster with singles, doubles, and perturbative triples (CR-EOMCCSD(T)) and use these results to evaluate the performance of various range-separated exchange-correlation functional within linear-response (LR) and real-time (RT) TDDFT. These calculations are used to benchmark the performance of various range-separated exchange-correlation functionals implemented within linear response and real-time TDDFT. Then time-dependent semi-empirical methods like TD-PM3 and TD-ZINDO were used since they are capable of handling very large systems. Once these semiempirical methods are reparamatized to match the CR-EOMCCSD(T) results, TD-ZINDO becomes roughly as accurate as range-separated TDDFT. Therefore, with proper parameterization, TD-ZINDO becomes roughly as accurate as range-separated TDDFT, at a fraction of the computational cost. Therefore TD-ZINDO is a capable of modeling the excitations in large poly-aromatic hydrocarbons, where modeling with coupled cluster or even TDDFT for these large systems is unfeasible.

L_a state (B_{2u}):optically very weak Dipole along short axis; bright.

N	CAM-B3LYP	CAM-B3LYP(2)	LC-BLYP	BNL	Iterative TDZINDO 1.267,0.64	Expt
2 Naphthalene	4.64	4.81	4.77	4.86	**4.59**	**4.66**
3 Anthracene	3.51	3.71	3.66	3.72	**3.55**	**3.60**
4 Tetracene	2.75	2.95	2.91	2.94	**2.85**	**2.88**
5 Pentacene	2.21	2.4	2.37	2.39	**2.37**	**2.37**
6 Hexacene	1.82	2	1.99	2	**2.03**	**2.02**
7 Heptacene	1.52	1.7	1.69	1.7	**1.77**	-

L_b state (B_{3u}) : Optically active (~100 times more than L_a) dipole along long axis; dim.

N	CAM-B3LYP	CAM-B3LYP(2)	LC-BLYP	BNL	Iterative TDZINDO 1.267,0.7	Expt
2	4.59	4.68	4.58	4.64	**4.21**	**4.13**
3	4.02	4.09	4.02	4.07	**3.67**	**3.64**
4	3.64	3.71	3.65	3.7	**3.32**	**3.39**
5	3.38	3.44	3.39	3.44	**3.10**	**3.12**
6	3.2	3.25	3.21	3.26	**2.96**	**2.87**
7	3.06	3.1	3.07	3.12	**2.82**	-

Table 0.1. Comparison of calibated TD-ZINDO method to experimental values and DFT using POL1 basis set with various functionals (all values in eV). TD-ZINDO with proper parameterization becomes roughly accurate as range-separated TDDFT, at a fraction of the computational cost making it capable of modeling large systems

Reference

[1] H. Hoppe and N. S. Sariciftci, Organic solar cells: An overview, Journal of Materials Research 19, 1924 (2004).

[2] M. A. Green, K. Emery, Y. Hishikawa, W. Warta, and E. D. Dunlop, Solar cell efficiency tables (version 39), Progress in Photovoltaics: Research and Applications 20, 12 (2012).

[3] R. A. J. Janssen and J. Nelson, Factors limiting device efficiency in organic photovoltaics, Advanced Materials 25, 1847 (2013).

[4] I. N. Levine, Quantum Chemistry*,* Prentice Hall, New Jersey, Ed 5th, (2001).

[5] A Szabo, N S Ostlund, Modern Quantum Chemistry Introduction to Advanced Electronic Structure Theory*,* Dover Publications, New York, (1996).

[6] R. G. Parr, W Yang, Density Functional Theory of Atoms and Molecules*,* Oxford University Press, New York, (1989).

[7] S. Hirata, M. Head-Gordon, Chem Phys Lett 302, 375 (1999).

[8] D. Neuhauser, R. Baer, J Chem Phys 123,204105 (2005).

[9] R. Baer, D. Neuhauser, J Chem Phys 121**,** 9803 (2004).

Chapter 1

Direct Delocalization for Calculating Electron Transfer in Fullerenes

A method is introduced for simple calculation of charge transfer between very large solvated organic dimers (fullerenes here) from isolated dimer calculations. The individual monomers in non-centrosymmetric dimers experience different chemical environments, so that the dimers do not necessarily represent bulk-like molecules. Therefore, we apply a delocalizing bias directly to the Fock matrix of the dimer system, and verify that this is almost as accurate as self-consistent solvation. Since large molecule like fullerenes have a plethora of excited states, the initially excited state orbitals are thermally populated, so that the rate is obtained as a thermal average over Marcus thermal transfers.

1.1 Introduction

Organic solar cells have gained much attention lately as an inexpensive alternative to inorganic cells, as they are getting closer to being economically viable.[1] However, little is understood about what fundamentally makes one type of organic solar cell more efficient than another.[2-3] One main bottleneck in many solar cells is the extraction of free electrons, i.e., even if the electron-hole separation is facile the diffusion of the free electrons to the electrodes could be a limiting factor.[4] This issue is especially important in fullerene based solar cells. In this study we therefore study electron transfer of several fullerene derivatives of the type most commonly used as electron acceptors in organic solar cells, and present a simple method for calculating the transfer rates.

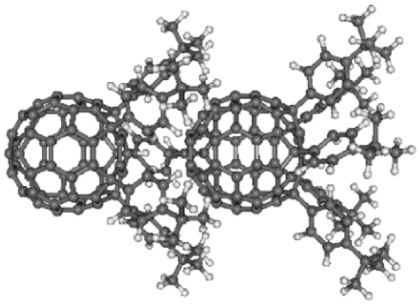

Figure 1.1: TBP dimer. Note the "cap" on the left molecule is exposed, whereas the cap on right molecule is solvated by the adducts of its neighbor.

The most popular electron acceptors in organic photovoltaic devices (OPVs) are fullerene derivatives, most notably [6,6]-phenyl-C_{61}-butyric acid methyl ester (PCBM).[5] Due to the large size of fullerenes molecules, it is necessary to apply a computationally efficient method for the study of transfer rates. In recent works we advocated a simple methodology for calculating the coupling between identical molecules in dimeric systems of fullerene derivatives.[6] In spite of the fact that the dimers are chemically identical, when they are not placed in a centrosymmetric fashion the chemical environment seen by each of the individual molecules is different (e.g., see Figure 1.1). Because of this, the order of the frontier orbitals involved in electron transfer (primarily the LUMO and LUMO+1 orbitals) could be misplaced; for example, in an isolated dimer calculation (where no delocalizing potential is applied), both LUMO and LUMO+1 could be located on the same molecule. In that case, a dimer calculation will show little transfer between the molecules.

To overcome the different-environment problem in isolated dimer calculations, we delocalize the LUMO and LUMO+1 across the two molecules using one of two methods. The first method involves "solvating" the dimer with surrounding molecules. Because the systems are so large, it would be too computationally expensive to explicitly treat solvating molecules; therefore we solvate the dimer with point charges. The values of the point charges are set self-consistently to equal the Mulliken charges on the atoms of the dimer. Solving for the values of the point charges is relatively arduous, so we have also shown that the same results can be achieved by applying an electric field to the system to delocalize the frontier orbitals. This method, which we label Delocalizing Field, is

much simpler in that one can sweep across a wide range of electric fields to see where the ideal delocalization occurs. However, due to the cost of density functional theory (DFT) simulations on large molecules, the delocalizing field method, while more simple than solvation, is still computationally expensive because it involves a potentially large number of DFT calculations.

We present a substantially more efficient method here. Rather than delocalizing the frontier orbitals with an electric field, we perform a single DFT calculation on a dimer system (here using the B3LYP functional). We then apply a bias directly to the post-self-consistent field (SCF) Fock matrix until the extra electron is balanced evenly between the two molecules in the dimer. We are then able to calculate the transfer rate according to Marcus theory. We show that the new method gives similar results and identical trends to the more complicated methods mentioned above.

The balance of the paper is as follows. We present a more detailed description of the methodology in Section II; results follow in Section III, and discussion in Section IV.

1.2 Methodology

Typically, the electron transfer rate is calculated for symmetric organic molecules from the Marcus theory expression,

$$k_{MT} = \frac{2\pi}{\hbar} \left|J_{ij}\right|^2 (4\pi\lambda\kappa_B T)^{-\frac{1}{2}} \exp\left(\frac{\left(\Delta E_{ij} + \lambda\right)^2}{4\lambda\kappa_B T}\right) \tag{1.1}$$

where "i" and "j" denote the initial and final states, located on the donor and acceptor, respectively, J is the transfer integral, ΔE_{ij} is the energy difference between the initial and final states, and λ is the reorganization energy. This expression is appropriate when the electronic states within both the

donor and acceptor are well-isolated; however, for large molecules such as fullerenes the distance between electronic states in the valence band is quite small, below 0.1 eV, so that a sum over all initial excited states is required; these initial states will each have its own rearrangement energies due to different coupling to the environment vibrational states. Further, in large molecules one does not really calculate the true electronic states but instead uses a single particle (or RPA/ TDDFT) approximation, making the degrees of freedom of the other electrons into an effective bath (not necessarily linearly coupled); these can actually enhance the transfer for symmetric systems, unlike vibrational degrees of freedom.

Here we therefore use a modified Marcus formalism,[7] whereby we sum over all initial states to calculate the total electron transfer rate:

$$k'_{MT} = \frac{2\pi}{\hbar}\sum_{ij} f(\epsilon_i - \mu_L)\left|J_{ij}\right|^2 (4\pi\lambda\kappa_B T)^{-\frac{1}{2}} exp\left(\frac{\left(\Delta E_{ij} + \lambda\right)^2}{4\lambda\kappa_B T}\right) \tag{1.2}$$

where we introduced the Fermi Dirac occupation of the donor states, defined as

$$f(\epsilon_i - \mu_0) = \frac{1}{1 + e^{\beta(\epsilon_i - \mu_0)}} \tag{1.3}$$

and ϵ_i is the energy of the donor state. In practice we report the rate in terms of the transfer time, defined as

$$\tau = \frac{1}{k'_{MT}} \tag{1.4}$$

For the most part, Eq. (1.2) is a straightforward generalization of the Marcus formula for a single pair of states. However, as stated above, each of these combinations of donor and acceptor states should in principle have a particular rearrangement energy. It is computationally demanding to calculate the reorganization energies for all the initial states, and the whole concept of transfer energy becomes questionable when there many low lying states, so to simplify we calculate the transfer rates for a range of values. According to MacKenzie et al,[8] the rearrangement energy for electron transfer in $C_{61}H_2$, i.e. a fullerene with the same linker group as PCBM, was calculated to be 0.136 eV when ignoring the outer sphere contribution to the reorganization. We therefore present results for which the reorganization energy was assumed to 0.1 eV and 0.15 eV. These choices bracket the relevant range of values, and take into account minor differences in the individual couplings and in the outer sphere contribution. While solvent effects are certainly important in electron transfer processes, for computational efficiency, we rely on the reorganization term in the Marcus theory formalism to account for these effects based on prior use of Marcus theory in electron transfer of large molecules (see Ref. 8, for example).

The computationally non-trivial aspect of the calculation is the transfer integral. Formally, the flux-operator has the form:

$$\tilde{J} = i[\tilde{F}, \tilde{\theta}] \tag{1.5}$$

where we introduced the Fock operator and the left-theta operator (identity on the left-fragment space, zero on the right); the tilde symbol on the matrices indicates that they refer to an orthogonal basis.

In practice, the calculations are performed by first generating the Fock and overlap matrices, F and S in a non-orthogonal basis using DFT, which has been shown to give good accuracy within the Marcus framework.[9-14] The NWChem software package was used for calculations.[15] The matrices were calculated using the B3LYP functional and STO-3G basis set for neutral and anionic systems. Results for both neutral and anionic system were similar (i.e., the choice of which Fock operator was used is immaterial in this basis set), and in the results section we use the neutral systems and anionic systems in PCBM, which are in good agreement, and the neutral systems for the other molecules.

The Fock matrix and theta operator are then converted to a local orthogonal basis:

$$\tilde{F} = S^{-\frac{1}{2}} F S^{-\frac{1}{2}}$$

$$\tilde{\theta} = S^{-\frac{1}{2}} \tilde{\theta} S^{-\frac{1}{2}} \tag{1.6}$$

and the theta operator determines whether the orbital of interest is on the left or the right molecule:

$$\theta_{ij} = g(i) S_{ij} g(j) \tag{1.7}$$

where

$$g(i) = \begin{cases} 1 \; if \; i \in \; left \; (donor) fragment \\ 0 \; otherwise \end{cases} \tag{1.8}$$

We then self-consistently calculate the chemical potential of the neutral and charged species, μ_0 and μ_{-1}, such that the following conditions are met:

$$2Tr\left[f\left(\tilde{F} - \mu_0\right)\right] = \sum_{j=1}^{N_o} f\left(\epsilon_j - \mu_0\right) = N$$
$$2Tr\left[f\left(\tilde{F} - \mu_{-1}\right)\right] = N + 1 \tag{9}$$

where N is the number of electrons in the neutral system, N_o is the number of orbitals and *f* is now a Fermi-Dirac operator

$$f\left(\tilde{F} - \mu_0\right) = \frac{1}{1 + e^{\beta\left(\tilde{F} - \mu_0\right)}} \tag{1.10}$$

The factor 2 in Eq. (1.9) above is due to spin.

We then apply a local bias *w* to the Fock matrix,

$$\tilde{F} \rightarrow \tilde{F} + w\tilde{\theta} \tag{1.11}$$

such that the extra electron is delocalized evenly between the two fragments. This is essentially the same as applying an external electric field on the system; however, as mentioned, there is significant time saving since the DFT calculation is only done once, post SCF convergence.

To calculate the transfer integral, we convert the theta operator into the molecular orbital basis,

$$\tilde{\theta}^E = V^T \tilde{\theta} V \tag{1.12}$$

where V is the eigenvector matrix of the orthogonal-basis Fock matrix, $\tilde{F}$. The transfer integral becomes:

$$J_{ij} = \left(\epsilon_i - \epsilon_j\right) \tilde{\theta}_{ij}^{E} \tag{1.13}$$

The transfer integral is then used to calculate the extended Marcus-theory rate, Eq. (1.2), summing over all initial states.

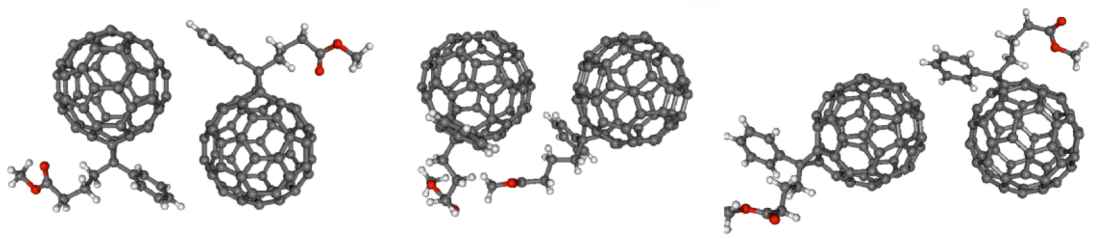

Figure 1.2: The three PCBM orientations studied in this paper, denoted in the results section PCBM-1, PCBM-2, and PCBM-3.

1.3 Results

We have studied several molecules, as follows: PCBM (Fig. 2), penta-(p-t-butylC_6H_4)-1-hydro-C_{60} (denoted TBP) (Fig. 1.1), and pentamethyl-monohydro-C_{60} (denoted $C_{60}Me_5H$) (Fig. 3). PCBM is the most commonly used fullerene in organic solar cells, and consists of a phenyl group and butyric acid methyl ester group attached to the fullerene ball via a methano-linker. Here, we study three dimer orientations of PCBM, each derived from a crystal structure. TBP and $C_{61}Me_5H$ are penta-substituted fullerenes, with tert-butyl phenyl and methyl adducts, respectively; each has an additional hydrogen atom bonded to the fullerene ball to compensate for the breaking of a double bond. The

allure of these molecules from a device fabrication perspective is that they tend to self-assemble into columns, which could enhance optimal phase separation in bulk heterojunction solar cells.

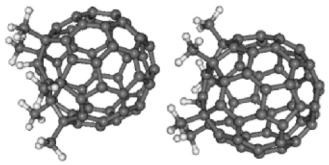

Figure 1.3: $C_{60}Me_5H$ dimer.

We present data for the extended Marcus theory formalism, that is, summation over all initial states (labeled as "multiple-state transfer time", as well as the traditional Marcus theory formalism, which typically only considers the coupling between the lowest states (LUMOs) on the left and right, which in our language amounts to including only the *i,j* = LUMO, LUMO+1 (and vice versa) in the sum in Eq. (1.2).

TABLE 1.1 Results of transfer times with the present formalism. Note the "cap" on the left molecule is exposed, whereas the cap on right molecule is solvated by the adducts of its neighbor.

Reorganization energy:	λ = 0.1 eV		λ = 0.15 eV	
Dimer:	Mutliple-state transfer time (fs)	LUMOs transfer time (fs)	Mutliple-state transfer time (fs)	LUMOs transfer time (fs)
PCBM-1	335	531	527	950
PCBM-2	322	1710	478	3060
PCBM-3	147	170	251	305
TBP	140000	773000	220000	1370000
$C_{60}Me_5H$	24200	33800	43200	60500

The results for the transfer time, τ, with the present formalism for the alignment potential w (i.e. satisfying Eq.(1.9)) are shown in Table 1.1. Note that in the table we refer to "Multiple-state transfer time", and to "LUMO-transfer time"; these refer to the inverse of the rates in Eqs. (1.2) and (1.1), respectively.

Table 1.2 presents the electron transfer times for PCBM where we calculated the Fock using several methods: neutral system with B3LYP functional, neutral system with PBE functional, and anionic system with PBE functional (we ignore the anionic system with B3LYP functional as B3LYP has been shown to give inadequate results for charged systems). The data shows similar results for the three methods, and in the interest of computational time, have shown results for neutral systems throughout.

Several things in particular stand out about the data. First, we demonstrate that for all the molecules presented a two-level Marcus formula is insufficient to fully capture the electron transfer behavior.

TABLE 1.2 Comparison of transfer times with neutral and anionic systems in PCBM.

Reorganization energy:	λ = 0.1 eV		λ = 0.15 eV	
Method	Mutliple-state transfer time (fs)	LUMOs transfer time (fs)	Mutliple-state transfer time (fs)	LUMOs transfer time (fs)
B3LYP neutral	335	531	527	950
PBE neutal	370	747	595	1300
PBE anionic	433	1100	680	2000

This is because for very large molecules such as fullerene derivatives, the excited states are sufficiently low that they can be thermally excited. Therefore, many levels can be thermally populated and can contribute to electron transfer.

We also note that for all relative orientations of PCBM, shown in Fig. 1.2, electron transfer rates

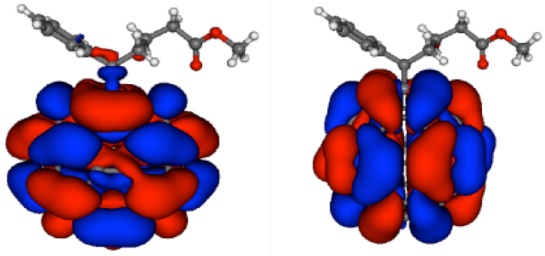

Figure 1.4: Frontier orbitals of PCBM. The LUMO is shown on the left, and LUMO+1 on the right.

are very high. Due to the spherical symmetry of the LUMO and LUMO+1 orbitals about the fullerene units in PCBM (shown in Fig. 1.4), the molecule conducts well in a variety of directions, and the rate of transfer is primarily a function of separation between these units. The variation in transfer times and the importance of summing over all initial states is primarily a result of the energy difference between the higher order state and the LUMO. For example, only a minor improvement in transfer time is seen in the third PCBM dimer; in this system, the LUMO+1 and LUMO+2 orbitals are 0.04 eV and 0.12 eV above the LUMO, respectively. Therefore, the standard Marcus transfer handles this system quite well. Alternatively, in the second PCBM dimer, the LUMO+1 and LUMO+2 are 0.07 eV and 0.10 eV above the LUMO. This energy difference results in a much more substantial contribution from the LUMO+2.

TABLE 1.3 Results for the variety of methods for TBP

Reorganization energy:	λ = 0.1 eV		λ = 0.15 eV	
Dimer:	Mutliple-state transfer time (fs)	LUMOs transfer time (fs)	Mutliple-state transfer time (fs)	LUMOs transfer time (fs)
Solvated TBP	84000	3500000	141000	6220000
Electric Field Delocalization	128000	1120000	208000	1980000
Direct Delocalization	140000	773000	2200000	1370000

The results for the variety of methods for TBP is shown in Table 1.3. Comparing the three methods, we note that the total solvation method gives transfer rates about 40% faster than the electric field delocalization and direct delocalization, which give very similar results. This is a result of several things. First, the addition of solvating molecules causes the frontier orbitals to have a much greater

overlap, i.e., the LUMO,LUMO+1 matrix element of the theta operator in the molecular orbital basis is much larger. Second, in the solvation method, the higher order frontier orbitals are closer to the LUMO than in the electric field and direct delocalization methods. For example, in direct delocalization, the LUMO+1 and the LUMO+2 are 5.94 x 10^{-4} eV and 3.06 x 10^{-2} eV above the LUMO, respectively; whereas when solvated, these orbitals are 5.10 x 10^{-4} eV and 2.57 x 10^{-2} eV above the LUMO. Additionally, excited states higher than the LUMO+2 play only a minor role in electron transfer, as the energy gap above the LUMO prevents significant population. We also note that the transfer times are also more greatly enhanced when one compares the multiple-state method to the LUMOs method. This is due to the higher level orbitals being closer to the LUMO. While the results presented for the several methods for calculating transfer times in TBP vary, we would argue that the solvation method provides the most accurate treatment of the system. The presence of point charges around the dimer, while not explicit treatment of neighboring molecules, most thoroughly mimics the bulk environment of the system. Nonetheless, the direct delocalization method provides a qualitative picture for comparing possible performance device of a number of molecules.

We also investigated the solvent effects of using the polarizable continuum model to solvate a TBP dimer, using the COSMO method in NWChem. We find that similar to calculations on an isolated dimer, the excited state orbitals are localized on a single fragment, and therefore no electron transfer is observed. We believe that this unphysical, and that the polarizable continuum model does not sufficiently capture the electronic behavior of the system. To compare the transfer rates of such a system, we applied the direct delocalization method, and find that the multiple-state transfer times are 133000 fs and 210000 fs for reorganization energies of 0.1 eV and 0.15 eV, respestively. This is in good agreement with our direct delocalization times of the unsolvated dimer.

1.4 Conclusions

We present a simple method to efficiently calculate electron transfer rates between molecular dimers. The method handles vastly asymmetric-placed dimers, where each individual molecule sees a different chemical environment. Additionally, the method is useful in molecules for which higher excited states interact with the frontier orbitals of the system. The proposed method is also highly efficient, as it does not require additional DFT calculations.

Of the molecules studied, PCBM and TBP have been fabricated to make OPV devices. According to experiment, PCBM makes significantly more efficient devices than TBP, 5-6% power conversion efficiency (PCE) versus 1.5% for TBP. While our study does not take into account the morphological behavior of these molecules, it gives a good basis for the types of molecules that would make efficient devices. We mention in the Results section, for example, the spherical symmetry of the LUMOs about the fullerene cage provides multidirectional pathways for electron transfer.

The work presented indicates several important factors relevant in the design of fullerenes for the use of organic solar cells. First, the methano-substituted motif, as in PCBM, conducts electrons well due to the spherical symmetry of the frontier orbitals. Additionally, substitutional motifs that retain this spherical symmetry about the fullerene unit would also make for high transfer rates. We should note, however, that this would not necessarily lead to a top performing cell as the energetics would still need to match those of the electron donor. Nonetheless, the particular motif seems highly efficient.

References

1. Hoppe, H.; Sariciftci, N. S. *J. Mat. Res.* **2004**, 19, 1924-1945.
2. O'Regan, B.; Gratzel, M. *Nature* **1991**, 353, 737-740.
3. Stier, W.; Prezhdo, O. V. *J. Phys. Chem. B* **2002**, 106, 8047-8054.
4. Nelson, *J. Curr. Op.Solid State Mat. Sci.* **2002**, 6, 87-95.
5. Brabec, C. J.; Gowrisanker, S.; Halls, J. J. M.; Laird, D.; Jia, S.; Williams, S. P. *Ad. Mate.* **2010**, 22, 3839-3856.
6. Arntsen, C.; Reslan, R.; Hernandez, S.; Kilbride, D.; Lopata, K.; Govind, N.; Gao, Y.; Tolbert, S.; Schwartz, B.; Rubin, Y.; Nardes, A. N.; Kopidakis, N.; Neuhauser, D. *in preparation.*
7. Chidsey, C. E. D. *Science* **1991**, 251, 919-922.
8. R. C. I. MacKenzie, J. M. Frost and J. Nelson, *J. Chem. Phys.* **2010**, 132, 064904-064906.
9. Bredas, J.-L.; Beljonne, D.; Coropceanu, V.; Cornil, J. *ChemInform* **2005**, 36, 4971-5003.
10. Lemaur, V.; da Silva Filho, D.A.; Coropceanu, V.; Lehmann, M.; Geerts, Y.; Piris, J.; Debije, M. G.; van de Craats, A.M.; Senthilkumar, K.; Siebbeles, L. D. A.; Warman, J. M.; Brédas, J.-L.; Cornil, J. *J. Am. Chem.l Soc.* **2004**, 126, 3271-3279.
11. Wu, Q.; Van Voorhis, T. The Journal of Chemical Physics **2006**, 125, 164105-164109.
12. Stein, T.; Kronik, L.; Baer, R. *J. Am. Chem. Soc.* **2009**, 131, 2818-2820.
13. Liu, C.; Walter, D.; Neuhauser, D.; Baer, R. *J. Am. Chem. Soc.* **2003**, 125, 13936-13937.
14. Chen, H.; Ratner, M. A.; Schatz, G. C. *J. Phys. Chem. C* **2011**, 115, 18810-18821.
15. Valiev, M.; Bylaska, E. J.; Govind, N.; Kowalski, K.; Straatsma, T. P.; Van Dam, H. J. J.; Wang, D.; Nieplocha, J.; Apra, E.; Windus, T. L.; de Jong, W. A. *Comp. Phys. Comm.* **2010**, 181, 1477-1489.

Chapter 2

Electron Transfer with TD-Split, a Linear Response Time-Dependent Method

We present a simple method, time-dependent split (TD-Split) for A → B electron transfer by a TD evaluation of the lowest excitation energy from the ground state of the combined $(AB)^-$ system. As an example, we study transfer between substituted fullerenes, primarily PCBM. Electron transfer in such fullerene systems is important as it is often the bottleneck in organic solar cells. The TD-Split method is described in detail, including numerical linearization which reduces the number of required iterations, and comparison to other possible approaches. We also compare to other molecules such as $C_{60}Me_5H$, and find similar trends as experiment.

2.1 Introduction

Electron transport is an established problem which continues to attract significant attention as it is both seemingly simple and physically and technologically important. In fact many of the challenges associated with devices such as photovoltaic devices are due to electron transport[1], making theoretical guidance desirable. An example is transport between fullerenes, which is a bottleneck in several fullerene-polymer solar energy architectures.

For small molecules, the treatment of electron transport of the generic form $(A^-)+B \rightarrow A+(B^-)$ is, at least in principle, well established. Two potential surfaces are constructed as functions of molecular coordinates, representing the reactants and products. Transition occurs essentially at the transition state where both potentials are equal.

For larger systems such an approach is more challenging, primarily since it is difficult to establish potential surfaces. Static DFT (Density Functional Theory), can be used but it is often not accurate for electronically excited states. TD-DFT, Time Dependent-Density Functional Theory, is generally more appropriate for excitations, so it is tempting to use it also for transport.[2-6]

Both TD-DFT and DFT present other challenges, primarily in determining what is the proper initial and final state. Specifically, the fundamental electronic structure overlap integral in the Marcus formalism is the transfer integral:

$$J = \left|\left\langle \phi_A \left| H \right| \phi_B \right\rangle\right|^2 \tag{2.1}$$

which refers to the left and right (initial and final) states, and H is the coupling Hamiltonian. The fundamental challenge is to properly define such initial and final states. It is possible to use an isolating potential to define these states[3]. However, unless the system is extremely large, the localization of the charge on one side influences the charge distribution on the other side, thereby influencing the transport; i.e., once the localization constraint is removed, then even when the charge is not yet transported from reactant to product (A to B in our example), there will be significant charge relaxation in both reactant and product and therefore apparent dynamics which is not due to the actual electron transfer, but has to do with the removal of the localization constraint.

In this paper we therefore present a different approach, which is inherently linear-response[7, 8] in form. The linear response nature of the method is numerically useful, as discussed later. We label the method TD-Split.

TD-Split is based on a response formula of the generic form:

$$\delta A(t) \equiv \left\langle \Psi(t) \left| A \right| \Psi(t) \right\rangle, \tag{2.2}$$

where $|\Psi(t)\rangle$ is a perturbed ground state of the complete system (i.e., with the electron delocalized over the donor and the acceptor); A is a perturbation operator as defined below. This formula has the inherent advantage that it has a very well defined initial state and any time-dependent dynamics is directly associated with the transport.

Physically, in the TD-Split approach, the initial state is the ground static density matrix associated with the whole (donor+acceptor) charged system. A time-dependent excitation is then applied; the response to this excitation peaks at a frequency which together with its amplitude determines the electron transfer rate. This approach is therefore inherently a linear response method, so that practically the very efficient numerical tools developed for linear response in time-dependent approaches are immediately useable.

The fundamental attraction in using the simple transport formula based on a symmetric case rather than a localized approach is apparent if we qualitatively view the system as a single electron being transported while the others act as a background. In this way of viewing the system, the initial state can be viewed as an electron transition-state, i.e., all the electrons arrange themselves so that one electron delocalizes as much as possible over the whole system.

The approach presented here is simplest to understand and to apply in a case where there is an isolated single pair of conducting molecular orbitals (i.e., with significant amplitude on the acceptor and donor). This case is very common in many practical applications, such as transport (hopping) between fullerenes or other symmetric or quasi-symmetric molecules. The method is however quite general to apply and will be useful in other circumstances, as explained below. For other time-dependent approaches in this context, see references [9-11].

The linear-response simulations use here a semi-empirical approach, TD-PM3 (Time Dependent-Parametric Model 3) [12]. An attractive feature of TD-PM3 is that as in TD-HF (Time-Dependent Hartree Fock), TD-PM3 has no self-energy in explicit open shell treatment, and reduced self-energy in a closed shell treatment. TD-PM3 is very efficient, both in scaling and in the use of a minimal basis set, and allows the treatment of realistic large organic systems. The methodology is general and applicable to other methods, primarily TD-DFT, which we plan to pursue in future work.

Several methods for extracting the information are discussed. In addition to direct time-dependent simulations, we discuss time-dependent linear response using Chebyshev propagation. Within the latter method, significant savings result when we use Filter-Diagonalization, which is a method for extracting frequency-resolved information from a short-time section of the results (or, in the Chebyshev case, from few iterations). The need for the method is especially acute in weakly coupled homogenous systems, because the splitting can be small so that a direct propagation or iterative methods would require long propagation times (as the propagation time is, in most methods, proportional to the inverse of the splitting). We show that with Filter-Diagonalization, few iterative steps (few thousands at most) are required.

The main example used here is a dimer of PCBM molecules. PCBM ([6,6]-phenyl-C61-butyric acidmethyl ester) has been the primary fullerene acceptor in organic solar cells for more than a decade; a dimer of PCBM molecules has a fairly large coupling of the LUMO levels of each PCBM. In addition to the PCBM dimer, we also investigated another example, transport within a $C_{60}Me_5H$ dimer.

In the remainder of the paper we discuss the propagation approaches (Section 2.2), discuss the numerical techniques used for the presented method (Section 2.3), and show sample results (Section 2.4) on PCBM and $C_{60}Me_5H$. Conclusions follow in Section 2.5.

2.2 Theory

2.2.1 Simplified Treatment

One approach for electronic transport is to apply a voltage or a bias in order to hold an electron or a portion of it in one of the molecules[13]. The bias is then relaxed and the change in charge distribution over both molecules is examined over time. This method will be referred to as release of bias.

Another method is derived from a simpler one-body problem where a single electron is transferred from a left molecule (donor) to a right molecule (acceptor). In a localized basis (left and right) the Hamiltonian governing this simple system is:

$$H = \begin{pmatrix} \varepsilon_L & \eta \\ \eta & \varepsilon_R \end{pmatrix}, \tag{2.3}$$

where ε_L is essentially equivalent to the energy of the LUMO in the left molecule (ϕ_L) and ε_R is associated with energy of the LUMO in the right molecule (ϕ_R).

The eigenvalues of the Hamiltonian are denoted as λ_+ and λ_-, associated with the symmetric and antisymmetric orbitals. The symmetric (+) and antisymmetric (-) eigenstates of the combined system can be described as combinations of ϕ_L and ϕ_R as follows:

$$\begin{aligned} \psi_+ &= a\phi_L + b\phi_R \\ \psi_- &= b\phi_L - a\phi_R \end{aligned} \tag{2.4}$$

which are normalized so $a^2+b^2=1$, and equivalently:

$$\begin{aligned} \phi_L &= a\psi_+ - b\psi_- \\ \phi_R &= b\psi_+ + a\psi_- \end{aligned} . \tag{2.5}$$

The coefficients *a* and *b* indicate how localized the transport is. If *a* and *b* are the same, then the molecular orbitals are very delocalized; but if $a=1$ and $b=0$, then there is no delocalization and there will be very little transport. As long as ε_L and ε_R are different by less than the coupling strength, *a* and *b* will be reasonably large. In that case, good electron transport is determined through having a large coupling strength. For degenerate initial states, the coupling is determined from η:

$$\gamma = \lambda_+ - \lambda_- = 2\eta \tag{2.6}$$

The splitting can be obtained by calculating the static energy difference between the two eigenstates.

The straightforward extension of this approach to interacting electronic systems uses the neutral combination (AB), and determines the splitting between the LUMO and LUMO+1 so that both levels are unoccupied and there is no inconsistency to the treatment. This method will be referred to as static-split.

2.2.2 TD Excitation

Finally, we suggest to obtain the splitting γ from a TD treatment, rather than from the static splitting. To obtain a time-dependent expression for γ, we revert back to the one-electron problem. The transition can be viewed as starting a wavefunction in one molecule and watching the transition to the other molecule; fundamentally this will then be:

$$Q(t) \equiv \left| \left\langle \phi_L \middle| \phi_R(t) \right\rangle \right|^2 . \tag{2.7}$$

The time-evolution of the symmetric and antisymmetric eigenstates is:

$$\begin{aligned} \left|\psi_{+}(t)\right\rangle &= e^{-i\lambda_{+}t}\left|\psi_{+}\right\rangle \\ \left|\psi_{-}(t)\right\rangle &= e^{-i\lambda_{-}t}\left|\psi_{-}\right\rangle. \end{aligned} \tag{2.8}$$

Substituting into equation (2.7) and simplifying, we get:

$$Q(t) = 4a^2b^2 \sin\left(\frac{(\lambda_{+} - \lambda_{-})}{2}t\right). \tag{2.9}$$

A Fourier transform of *Q(t)* will give $\gamma/2$ by the location of the maximum and the magnitude will give $4a^2b^2$.

It is necessary to obtain a form that can be used with TD-PM3. This will be done by introducing the following:

$$B(t) \equiv \left\langle \psi_{+} \middle| \theta_L e^{iHt} \theta_R e^{-iHt} \middle| \psi_{+} \right\rangle \tag{2.10}$$

Here, θ_L and θ_R are step functions; θ_L is 1 on the left and 0 on the right, and the opposite for θ_R. Formally,

$$\begin{aligned} \theta_L \left|\phi_L\right\rangle &= \left|\phi_L\right\rangle \\ \theta_R \left|\phi_L\right\rangle &= 0 \\ \theta_L \theta_R &= 0. \end{aligned} \tag{2.11}$$

To verify that *B*(t) in equation (2.10) serves the same purpose as equation (2.7), we note that:

$$B(t) = \left\langle \psi_{+} \middle| \theta_L e^{(i(H-\lambda_{+})t)} \theta_R \middle| \psi_{+} \right\rangle. \tag{2.12}$$

Now let:

$$1 = \left|\psi_{+}\right\rangle\left\langle\psi_{+}\right| + \left|\psi_{-}\right\rangle\left\langle\psi_{-}\right|. \tag{2.13}$$

Inserting equation (2.13) into equation (2.12) gives:

$$B(t) = \langle \psi_+ | \theta_L \left(|\psi_+\rangle\langle\psi_+| + |\psi_-\rangle\langle\psi_-| \right) e^{\left(i(H-\lambda_+)t\right)} \theta_R |\psi_+\rangle, \tag{2.14}$$

so

$$\begin{aligned} B(t) &= \langle \psi_+ | \theta_L |\psi_+\rangle\langle\psi_+ | \theta_R |\psi_+\rangle \\ &+ e^{-i\gamma t} \langle \psi_+ | \theta_L |\psi_-\rangle\langle\psi_- | \theta_R |\psi_+\rangle . \end{aligned} \tag{2.15}$$

Substituting with equation (2.4) gives

$$B(t) = a^2 b^2 \left(1 - e^{i\gamma t}\right). \tag{2.16}$$

This is analogous to *Q(t)* and taking the Fourier transform of both will yield a similar spectrum of similar magnitude.

To make equation (2.10) more applicable for use in TD-PM3, it is written as

$$B(t) = \mathrm{Tr}\left(|\psi_+\rangle\langle\psi_+| \theta_L e^{iHt} \theta_R e^{-iHt} \right), \tag{2.17}$$

or:

$$B(t) = \mathrm{Tr}\left(P_0 \theta_L e^{iHt} \theta_R e^{-iHt} \right). \tag{2.18}$$

Here, P_0 is the initial density matrix taken in the symmetric state,

$$P_0 = |\psi_+\rangle\langle\psi_+|. \tag{2.19}$$

Eq. (2.19) is in a form that can be usable in TD-PM3 or TD-DFT. To turn it into a form that can be used with efficient numerical methods, first recognize that:

$$2i\,\mathrm{Im}\left(B(t)\right) = \mathrm{Tr}\left(\mathrm{P}_0 \theta_L e^{iHt} \theta_\mathrm{R} e^{-iHt} \right) - \mathrm{Tr}\left(e^{iHt} \theta_R e^{-iHt} \theta_L P_0 \right) \tag{2.20}$$

But since:

$$i\theta_L = \frac{\partial e^{i\alpha\theta_L}}{\partial \alpha}\Big|_{\alpha=0} \tag{2.21}$$

we get:

$$\mathrm{Im}\left(B(t)\right) = -\frac{1}{2}\frac{\partial \mathrm{Tr}\left(e^{-iHt}e^{-i\alpha\theta_L}P_0 e^{i\alpha\theta_L}e^{iHt}\theta_R\right)}{\partial\alpha}\Big|_{\alpha=0}. \tag{2.22}$$

To simplify, let:

$$P_\alpha(0) = e^{-i\alpha\theta_L}P_0 e^{i\alpha\theta_L}, \tag{2.23}$$

and also:

$$P_\alpha(t) = e^{-iHt}P_\alpha(0)e^{iHt}. \tag{2.24}$$

The above can then be inserted into equation (2.22) to become:

$$\mathrm{Im}\left(B(t)\right) = -\frac{1}{2}\frac{\partial \mathrm{Tr}\left(P_\alpha(t)\theta_R\right)}{\partial\alpha}\Big|_{\alpha=0}. \tag{2.25}$$

TD-PM3 or TD-DFT can be used to obtain the time evolution of $P_\alpha(t)$. The derivative with respect to α can be obtained using numerical methods. Some efficient numerical methods to be used are described in the next section.

2.3 Practical Evolution

Here we outline the practical evolution of the transmission.

2.3.1 Initial State

The first stage is the preparation of an initial ground state; for large systems, we will likely choose between Hartree-Fock, a semi-empirical method (PM3, etc.), or DFT, although the same formalism is useful if other methods, such as MP2, are applied to the ground-state calculation. Eventually, the ground state of the complete system density (P_0) or initial wavefunction/orbitals $|\Psi_0\rangle$ is obtained.

Next, a perturbation operator is found. In practice, several perturbation operators are potentially useful (possibly in combination, as described below). The first is θ_L from equation (2.11). A second is:

$$A = |\phi_L\rangle\langle\phi_L| - |\phi_R\rangle\langle\phi_R|. \tag{2.26}$$

A third option is simply:

$$A' = |\phi_{\text{homo}}\rangle\langle\phi_{\text{lumo}}| + c.c. \tag{2.27}$$

The last (third) transition operator will not yield the correct amplitude for the transitions (the equivalent of $4a^2b^2$) unless the system is close to symmetric, so a~b~$1/\sqrt{2}$.

2.3.2 Linear-Response Evolution

Next is the evolution in time. In the methods we consider the Fock operator is used to propagate a density matrix (or a set of orbitals); these methods includes TD-HF, TD-DFT, and TD-PM3. The details of the Fock operator depend on the method used; for TD-PM3, for example, see Ref.[14, 15], but briefly it is formally similar to Hartree-Fock:

$$F_{ij} = h_{ij} + \sum_{kl} V_{ijkl} P_{kl}, \tag{2.28}$$

except that now h_{ij}, V_{ijkl} are semiempirical matrix elements, and each V_{ijkl} vanishes unless it is a two center integral, i.e., the only non-zero elements are:

$$V(i_a, j_a, k_b, l_b),\ V(i_a, j_b, k_a, l_b),\ V(i_a, j_b, k_b, l_a), \tag{2.29}$$

where i_a, for example, refers to a basis function "i" localized on atom "a".

One option would have been to use explicit time-dependent propagation. Then, starting at P_0, include the perturbation to get:

$$P\left(t=0^{+}\right)=P_0-i\eta\left[A,P_0\right], \tag{2.30}$$

After that, propagate forward the Fock equation,

$$\frac{idP}{dt}=\left[F(P),P\right], \tag{2.31}$$

where F is the density-dependent Fock operator.

Another option pursued here, is to use the linear response time-dependent Chebyshev approach[7, 16]; briefly, in the approach one first constructs residues:

$$R_n=\mathrm{Tr}\left(BX_n\right), \tag{2.32}$$

where the modified Chebyshev series is defined as:

$$\begin{aligned} X_0&=-i\left[A,P_0\right]\\ X_1&=\frac{1}{\Delta H}LX_0\\ X_n&=\frac{2}{\Delta H}LX_{n-1}+X_{n-2}, \end{aligned} \tag{2.33}$$

and ΔH is a numerical parameter characterizing the spectrum of the Fock operator (typically chosen as ~75eV for TD-PM3 applications) and the Liouville operator is defined as:

$$LP=\frac{1}{\zeta}\left[F\left(P_0+\zeta P\right),P_0+\zeta P\right]-\left[F\left(P_0\right),P_0\right], \tag{2.34}$$

where ζ is a small number chosen to ensure the linear response; for clarity, we denote the explicit density dependence of the Fock operator.

From the modified Chebyshev series and the residues there are three options. One is to construct explicitly the time-dependent signal,

$$\delta B(t) = \sum_n (2 - \delta_{n0}) J_n (t\Delta H) R_n, \tag{2.35}$$

and then Fourier transform the above signal. A more efficient option is to directly Fourier transform the Chebyshev series elements, leading to

$$B(\omega) = \sum_n b_n (\omega) R_n, \tag{2.36}$$

where

$$b_n (\omega) = (2 - \delta_{n0}) \int_0^\infty e^{i\omega t} f(t) J_n (t\Delta H) dt, \tag{2.37}$$

and the damping function is

$$f(t) = e^{-\alpha t}. \tag{2.37}$$

2.3.3 Filter-Diagonalization

The third option for extracting the eigenvalues is Filter-Diagonalization[17]. Briefly, this is a method to expand a general series, C_n, as made from (initially unknown) complex frequencies and weights (ω_k, p_k) as:

$$C_n = \sum_k p_k e^{i\omega_k n} \tag{2.39}$$

In its most relevant form for this problem,[18] Filter-Diagonalization becomes an approach to extract the frequencies and weights directly from the Chebyshev series. Filter Diagonalization extracts the coefficients and eigenvalues directly from such a series in fewer terms than a Fourier transform will (i.e., with fewer elements than necessary in a series such as the one in equation (2.36) to develop well-isolated peaks). In this context, this is based on formally writing the initial modification to the density matrix (i.e., its linear response part) as:

$$X_0 = \sum_k p_k \Lambda_k \tag{2.40}$$

where each Λ_k is a separate density matrix that is an eigenstate of the Liouville operator, i.e.,

$$L\Lambda_k = i\lambda_k \Lambda_k \tag{2.41}$$

and

$$\mathrm{Tr}\left(\Lambda_k \Lambda_j\right) = \delta_{jk} \tag{2.42}$$

so

$$p_k = \mathrm{Tr}\left(X_0 \Lambda_k\right). \tag{2.43}$$

(Note that λ_k are the transition frequencies.) Then, each residue is formally:

$$R_n = \sum_k p_k \cos\left(n z_k\right) \tag{2.44}$$

where

$$z_k = \cos^{-1}\left(\frac{\lambda_k}{\Delta H}\right) \tag{2.45}$$

Equation (2.44) has the form of a harmonic series, i.e., a sum of a series of exponential terms.

For the present application, we note that Filter-Diagonalization can be further improved because of the structure of the eigenvalues. The eigenvalues of the Liouville operator come here in pairs of negative and positive imaginary values, i.e., for each positive λ_k there is a negative one. We are interested in the pair with the lowest $|\lambda_k|$, which we will denote as λ_{min}, $-\lambda_{min}$, each of which is associated with the HOMO–LUMO splitting frequency.

The usual Filter-Diagonalization technique will be challenged by the need to separate the pair of z's that are associated with λ_{min}, $-\lambda_{min}$, which we will denote as z_{min}, π-z_{min} (and z_{min} is close to $\pi/2$). To circumvent this, we note that because of the pairing of the negative and positive eigenvalues, the odd terms will vanish

$$0 = R_1 = R_3 = \ldots = R_{2n+1} \tag{2.46}$$

So that we define a new series

$$Q_n = R_{2n}, \quad n = 0,1,2,\ldots \tag{2.47}$$

and then use Filter-Diagonalization to fit it to

$$Q_n = \sum_k 2p_k \cos\left(2nz_k\right), \tag{2.48}$$

where now the sum is over half the eigenvalues, i.e., the z_k associated with positive λ_k. With this slight modification, Filter-Diagonalization is much more effective as it does not need to separate two very closely-spaced eigenvalues.

2.4 Results

The simulations were done on electron transport between two fullerene derivatives. The bulk of the simulations were done on a dimer of the PCBM fullerene derivatives. This system was constructed by taking a PCBM molecule and its nearest neighbor from the crystal structure of PCBM·1,2-$C_6H_4Cl_2$, as shown in Figure 2-1.[19] The PCBM dimer used here was chosen out of the other combinations in the crystal structure as it is relatively the closest, so its conductivity is assumed to be the highest of all the other combinations.

The rest of the simulations were done on a dimer of pentamethylmonohydro[60] fullerenes, which we will refer to as $C_{60}Me_5H$. The system was obtained by taking a molecule of $C_{60}Me_5H$ and

its nearest neighbor in a head-to-tail stacked arrangement from the crystal structure of $C_{60}Me_5H \cdot CS_2$,[20] as shown in Figure 2-2. The $C_{60}Me_5H$ dimer was chosen as it provides a simple example of the stacking motif often observed in pentaaryl fullerenes, which have previously been evaluated as acceptors in bulk-heterojunction photovoltaic devices. Arranged in such a way, the contiguous π-electron systems are well separated and the dimer is thus expected to have a lower conductance, thereby exemplifying weakly conductive systems.

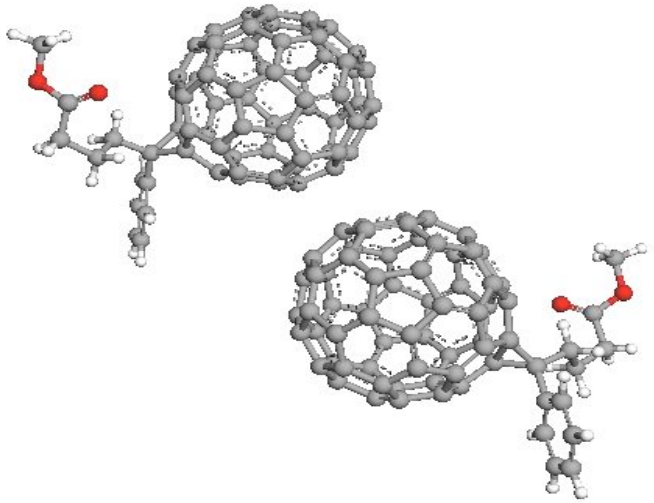

Figure 2-1: PCBM dimer

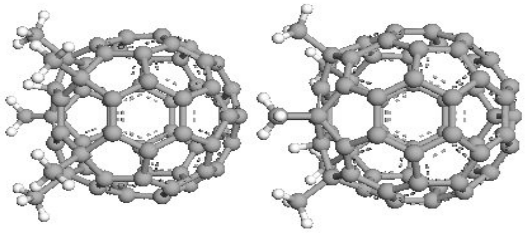

Figure 2-2: $C_{60}Me_5H$ dimer

As a first stage in all methods, the ground state was found using the PM3 program in the MOPAC[21] package. Simulations were done on the PCBM dimer at the natural distance of 10.1 Å determined from the crystal structure of PCBM·1,2-$C_6H_4Cl_2$ and also at stretched distances.

In the simplest approach, static splitting, the orbital eigenvalues for the ground state were used to calculate the differences between the LUMO and LUMO+1 of the neutral combination. One important point is that before calculation, it is necessary to ensure that the LUMO and LUMO+1 are extended, i.e., do not localize on the fragments; otherwise, the splitting will be high but there will be no transition. To ensure that the LUMO and LUMO+1 are delocalized, we apply a potential which is uniform on each fragment but is different between the fragments (similar results would have been obtained from applying an electric field). Such a potential is similar to a localization potential, but its role is to delocalize the orbitals. In practice, the value of the potential enters the Marcus formulae, i.e., it is essentially part of the rearrangement energy – which is defined by the point where the two fragments have the same potential energy (here where the potential is delocalized). Results of the static splitting approach shown in Figure 2-3.

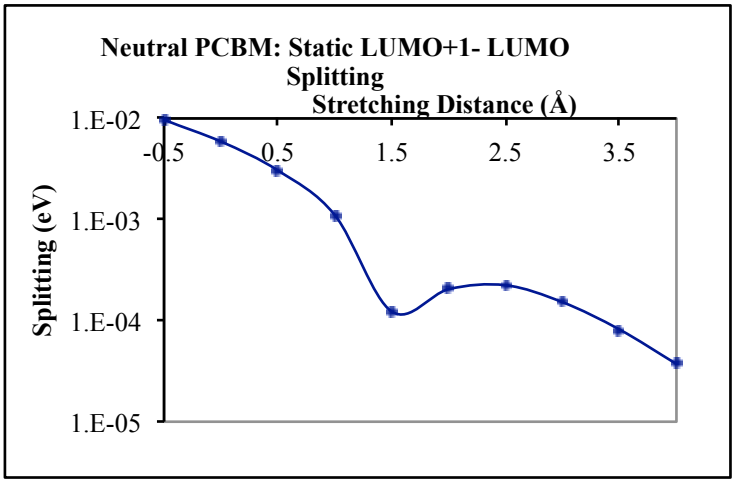

Figure 2-3: Static splitting for a stretched neutral PCBM dimer as a function of extra stretching distance "0" refers to the equilibrium distance; other distances refer to pushing or stretching the fragments away.

Next we show the results of calculating the time-dependent transmission by biasing the molecule, releasing the bias, and following the actual transfer of the electron (release of bias method).

Specifically, first we obtain the ground state of the system in an ionic state using PM3 in the MOPAC package, with an extra electron inputted in the LUMO of the system. A bias is then applied and then released. The PCBM system is run with two choices:

- A bias that is large enough to initially keep the extra electron in one of the molecules and:
- A small bias that initially keeps 60% of the extra electron in one of the molecules and 40% in the other.

Simulations were done on the PCBM system with the natural and stretched distances. The trace of the electron density on the molecule that had the lesser density was calculated over time and shown in Figure 2-4.

Interestingly, for large bias the electron localizes, so that even after the bias is released the system does not fully oscillate (Figure 2-4). This is because the system is initially not in an electronic transition state; i.e., the electrons on each side adjust their orbitals in the presence of the bias, and the release of the bias does not sufficiently force the electrons to redistribute.

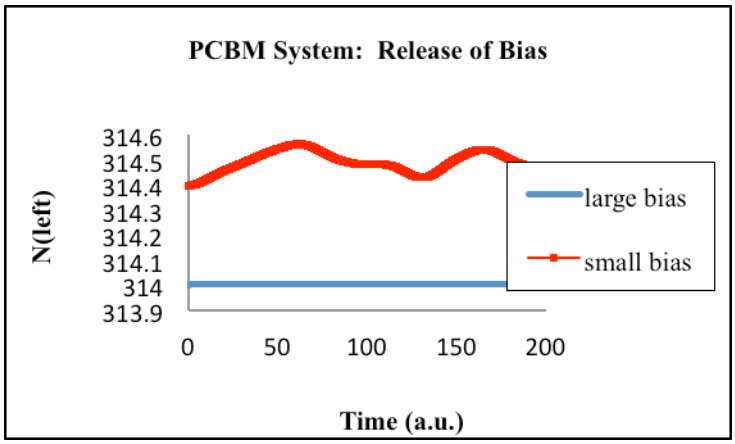

Figure 2-4: Trace of electron density using the bias release method

In spite of the localization of the electron, it is possible to extract a form of a transfer frequency by taking a Fourier transform of the results shown in Figure 2-4; the peak, as a function

of the distance between the PCBM molecules, is shown in Figure 2-5. As shown, the results depend on the bias. This is discussed in the conclusions below. However, since the amplitude of the oscillations is small, the frequency cannot be treated as a full electron oscillation.

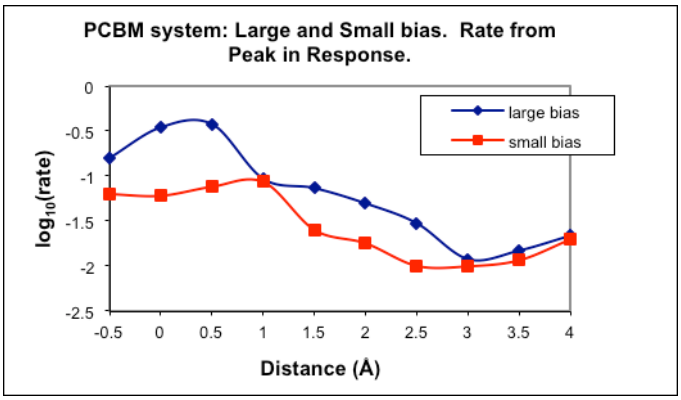

Figure 2-5: Transfer frequency (in eV) from extracting a bias and then releasing it, for the PCBM dimer, as a function of stretching distance ("0" refers to the equilibrium distance).

Finally, we turn to the main method discussed here, TD-Split, where TD-PM3 is used to extract the HOMO–LUMO splitting for the ionic state without applying a bias on the neutral molecule. First, PM3 (again from MOPAC) was used, without applying a bias, to calculate the ground state. TD-PM3 was then used to propagate Eq. (2.25). The previously described Chebyshev and Filter-Diagonalization approaches (Eqs. (2.32)–(2.48)) were used to obtain the results.

Both a direct Chebyshev propagation (Eq. (2.36)) and Filter-Diagonalization gave comparable results. For the Chebyshev approach we typically used 25000 iterations, while for Filter-Diagonalization typically 3000 total iterations were used. The Chebyshev method gives a continuous graph (Eq. (2.36)) of spectra vs. frequency, and the first peak yields the splitting, as shown in Figure 2-6. Filter-Diagonalization gives the results as discrete values.

The splitting determined from Chebyshev and Filter-Diagonalization is very similar, as shown in Figure 2-7; the only difference between the two methods is found for a weakly interacting

system, i.e., PCBM at very large distances where 25000 Chebyshev iterations are not sufficient for convergence, but Filter-Diagonalization with 3000 iterations is ample.

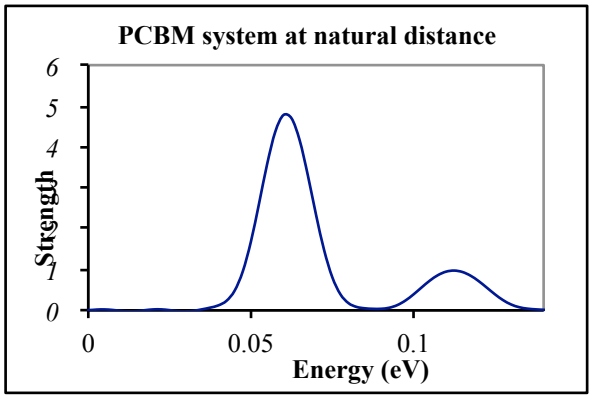

Figure 2-6: TD-Split HOMO–LUMO splitting for the charged PCBM system obtained with the Chebyshev approach (Eq. (2.36)).

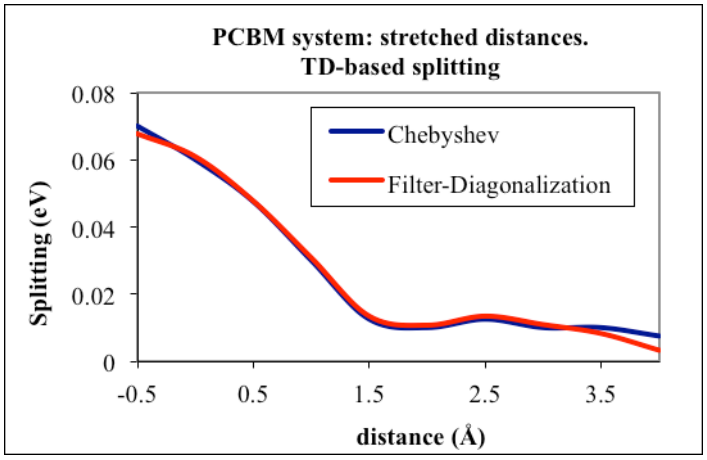

Figure 2-7: HOMO–LUMO splitting for a charged PCBM dimer system obtained using direct Chebyshev simulations (Eq. (2.36)) vs. Filter-Diagonalization using the Chebyshev residues (Eq. (2.44)).

Finally, these three methods discussed above are compared to each other in Figure 2-8.

The first method, static-split, involves finding the difference between the LUMO+1 and the LUMO of the neutral molecules. This method is simple in that only a static PM3 or DFT

calculation is required and so is the fastest. The results show that the splitting, and so the electron transfer, is reduced as the PCBM molecules are stretched apart, but is significantly smaller than the TD-PM3 results.

The second method, release of bias, which involves a bias that initially fixes the electron density and then releases it, generally follows the trend of decreasing conductance with increasing distance between the molecules, but the oscillation amplitude is too small when a large bias is used.

The third method, TD-Split, introduces TD-PM3 as a way to get the (charged-system) HOMO–LUMO split for the transferred molecule, from which we get the electron transfer rate. Similar methodology will work with TD-DFT. TD-PM3 allows for fast results, so the method can conceivably be used for combinatorial searches of improved transfer. Note that TD-Split can be considered as the limit of the 2nd approach (release of bias), when an infinitesimally small bias is used and then released.

Comparison with the first method (static split) shows that TD-Split gives significantly larger rates than the static version, at least when we used TD-PM3 and PM3. TD-Split best shows a trend of decreased electron transfer with increasing distance between the molecules. To further test the magnitude of the splitting produced by the TD-Split, simulations were done on $C_{60}Me_5H$ and are compared with those of PCBM. The results are shown in figure 2-9. The equilibrium distance of $C_{60}Me_5H$ is 10.0 Å. This graph shows how the $C_{60}Me_5H$ dimer has much lower TD-based splitting than PCBM dimer (where in both cases the systems are negatively charged, to represent the transferred electron).

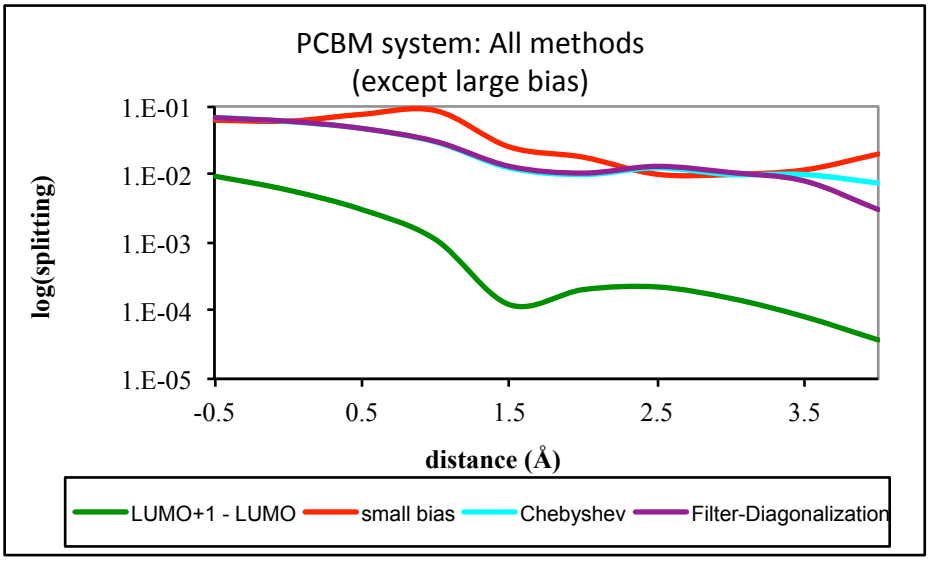

Figure 2-8: Comparison of all methods. "Chebyshev" refers to Eq. (2.36) and Filter-Diagonalization to Eq. (2.44). The most important feature of this figure is the large difference between the static approach (LUMO+1 to LUMO for a neutral system) and the linear response TD split approaches, which predict a much larger splitting (i.e., transfer).

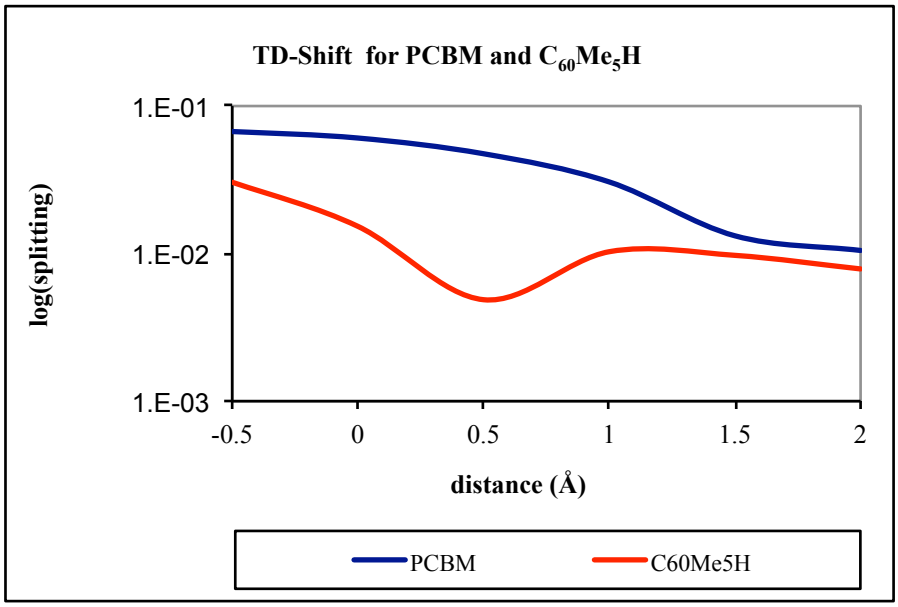

Figure 2-9: Comparison of TD-Split from Filter-Diagonalization for both systems: PCBM dimer and $C_{60}Me_5H$ dimer

2.5 Conclusions

We have presented a TD-method to studying electron transfer between two molecules, TD-Split. We used here TD-PM3 due to its speed over TD-DFT, but either TD-DFT or alternately any other semiempirical method beyond PM3 could be used. This method was also compared with two other methods to study electron transfer, static-split and release of bias, and showed larger rates and consistent decay with transfer distance.

Future work involves improving on this proposed method. One is to use open-shell TD-PM3, rather than closed-shell. This should eliminate any residual self-energy and its effects. Another potential improvement is to use this method with TD-DFT rather than TD-PM3.

An interesting variant will be to study the flux-flux evolution in time, and see how polarization and time-dependent effects influence it; i.e., how the other electrons in the molecule "solvate" the transferred electrons.

Finally, the technique allows quantitative studies of the efficiency of transfer in different organic systems, and will be used to suggest theoretical guidance on the experimental transport of electrons in fullerenes. A follow-up paper will tackle this problem.

2.6 Acknowledgements

We are grateful for help by members of the Solar EFRC UCLA group, including Ives Rubin, Ben Schwartz, Sarah Tolbert and their group members. We are also especially thankful to Ives Rubin for his useful comments on the manuscript. The research was supported by the DOE EFRC program.

References

[1] B. Oregan and M. Gratzel, *Nature,* **353**, pp. 737-740, 1991.

[2] T. Stein, L. Kronik, and R. Baer, *Journal of the American Chemical Society,* **131**, pp. 2818-2820, 2009.

[3] H. Eshuis and T. van Voorhis, *Physical Chemistry Chemical Physics,* **11**, pp. 10293-10298, 2009.

[4] C. Liu, D. Walter, D. Neuhauser, and R. Baer, *Journal of the American Chemical Society,* **125**, pp. 13936-13937, 2003.

[5] O. V. Prezhdo, W. R. Duncan, and V. V. Prezhdo, *Progress in Surface Science,* **84**, pp. 30-68, 2009.

[6] C. M. Isborn and X. Li, *The Journal of Chemical Physics,* **129**, pp. 204107-8, 2008.

[7] R. Baer and D. Neuhauser, *Journal of chemical physics,* **121**, pp. 9803-9807, 2004.

[8] C. M. Isborn and X. S. Li, *Journal of Chemical Theory and Computation,* **5**, pp. 2415-2419, 2009.

[9] R. Baer, *Chemical Physics Letters,* **364**, p. 75, 2002.

[10] A. Czader and E. R. Bittner, *Journal of Chemical Physics,* **128**, p. 035101 (12 pages) 2008.

[11] V. Chernyak, M. F. Schulz, S. Mukamel, S. Tretiak, and E. V. Tsiper, *Journal of Chemical Physics,* **113**, pp. 36-43, 2000.

[12] L. A. Bartell, M. R. Wall, and D. Neuhauser, *Journal of Chemical Physics,* **132**, p. 234106 (6 pages), 2010.

[13] R. Baer and D. Neuhauser, *Journal of chemical physics,* **125**, p. 074709, 2006.

[14] M. J. S. Dewar and W. Thiel, *Journal of the American Chemical Society,* **99**, pp. 4899-4907, 1977.

[15] M. J. S. Dewar and W. Thiel, *Theoretica Chimica Acta,* **46**, pp. 89-104, 1977.

[16] D. Neuhauser and R. Baer, *Journal of chemical physics,* **123**, p. 204105, 2005.

[17] M. R. Wall and D. Neuhauser, *Journal of chemical physics,* **102**, pp. 8011-8022, 1995.

[18] V. A. Mandelshtam and H. S. Taylor, *Physical Review Letters,* **78**, pp. 3274-3277, 1997.

[19] R. D. Kennedy, A. L. Ayzner, D. D. Wanger, C. T. Day, M. Halim, S. I. Khan, S. H. Tolbert, B. J. Schwartz, and Y. Rubin, *Journal of the American Chemical Society,* **130**, pp. 17290-+, 2008.

[20] T. Niinomi, Y. Matsuo, M. Hashiguchi, Y. Sato, and E. Nakamura, *Journal of Materials Chemistry,* **19**, pp. 5804-5811, 2009.

[21] J. J. P. Stewart, *Journal of Computer-Aided Molecular Design,* **4**, pp. 1-45, 1990.

Chapter 3

Electron Transfer Beyond the Static Picture:

A TDDFT/TD-ZINDO Study of a Pentacene Dimer

We use time-dependent density functional theory and time-dependent ZINDO (a semi-empirical method) to study transfer of an extra electron between a pair of pentacene molecules. A measure of the electronic transfer integral is computed in a dynamic picture via the vertical excitation energy from a delocalized anionic ground state. With increasing dimer separation, this dynamical measurement of charge transfer is shown to be significantly larger than the commonly used static approximation (i.e., LUMO+1 - LUMO of the neutral dimer, or HOMO - LUMO of the charged dimer), up to an order of magnitude higher at 6 Å. These results offer a word of caution for calculations involving large separations, as in organic photovoltaics, where care must be taken when using a static picture to model charge transfer.

3.1 Introduction

Accurately computing electron transfer rates and probabilities is crucial for understanding a wide range of devices and effects, including many types of chemical reactions[1, 2], solar cells[3, 4], nanoelectronics[5], and molecular electronics[6-9]. For example, in fullerene-based organic photovoltaics (OPVs), after photo-excitation of the light harvesting polymer, a charge-separated electron is first transferred to a nearby fullerene molecule, then subsequently shuttled to the electrode via a series of "hops" from one fullerene to another adjacent one. The success of an OPV often hinges on how readily electrons can be shunted from polymer to electrode without

recombination with a hole. In general, this is a function of both the device morphology and also the electron transfer probability between two fullerene molecules. Increasing device efficiencies by optimizing transfer between fullerene pairs (e.g., via functionalization) thus offers a tantalizing opportunity. Unfortunately, predictive calculations of transfer probabilities are often elusive as electron transfer in these systems is a complicated process involving coupling between electronic and nuclear motion, in addition to the coupling with environment.

Electron transfer calculations on model systems and simple analogues offer a path forward. There has been much recent progress in modeling electron transfer between isolated molecules. The electron transfer reaction $A^- B \rightarrow A B^-$ is well established in principle using Marcus Theory (for overview see Ref. [10]), where the transfer is computed in the non-adiabatic regime—i.e., weak electronic coupling between the donor and acceptor means that inter-conversion between from the donor to the acceptor diabatic potential energy surface can be computed semi-classically. Here, two potential surfaces (reactants and products) are required as functions of molecular coordinates, and the transfer probability is computed from three main ingredients: ΔG^0, the free energy difference between the two states; λ, the energy required to reorganize the system, possibly including a solvent shell, from initial to final state without actually transferring charge; and J, the electronic coupling between the initial and final states. While any number of theoretical approaches can be used within the Marcus framework (e.g., from semi-empirical to correlated methods), density functional theory (DFT) has been the most popular recently, due to good accuracy and modest computational cost[7, 9, 11-14].

For DFT, the main challenge lies in determining proper initial and final states in the transfer integral J in the Marcus formalism

$$J = |\langle \psi_F | H | \psi_I \rangle|^2,$$

where $|\psi_I\rangle$ and $|\psi_F\rangle$ are the initial and the final states, and H is the electronic coupling Hamiltonian (for more details, see review by Hsu[15]). Although at first glance straightforward, extreme care must be taken in choosing these states to avoid non-physical effects. For example, if one picks $|\psi_I\rangle = A^- B$ and $|\psi_F\rangle = A B^-$ the resulting dynamics could be dominated by electronic relaxation rather than charge transfer.

This issue of correct choice of initial and final states can be bypassed by simply comparing the LUMO and LUMO+1 of the neutral pair, which also gives a rough measure of the coupling (i.e., the larger the splitting the less the transfer probability). The picture, however, is only qualitative as in reality the transfer involves the coupling of a negatively charged molecule with a neutral one; this often consists of a significantly perturbed electronic structure from the neutral case.

For predictive calculations, however, the transfer integral J must be computed as accurately as possible, with proper choice of $|\psi_I\rangle$ and $|\psi_F\rangle$. To this end, we recently presented a new approach to electron transfer calculations named TD-Split, where the transfer integral is calculated using the vertical excitation energy of a negatively charged dimer from a fully delocalized ground state[16]; this excitation energy can be computed using virtually any time-dependent method. A related method is generalized Mulliken-Hush (GMH), which computes the coupling using the vertical excitation energy and transition dipole moment between two charge-localized states[17]. In TD-Split the nuclear degrees of freedom are frozen, the "reaction coordinate" is the degree of charge localization, and the resulting transfer integrals are associated with the rate of electron transfer for particular system geometry. This is contrast to traditional Marcus-type calculations, which includes the effect of the vibrational degree of freedom.

Marcus theory gives essentially the exact result (in the nonadiabatic limit) when the electronic transfer integrals are known. For large scale systems, where the transfer integrals are almost always calculated by DFT or Hartree Fock or semiempirical methods, most of the electronic degrees of freedom are frozen in the calculation. Put differently, the possibly crucial effect of the other electrons on the transfer is neglected in such single-particle static calculations, and TD Split corrects this omission. Therefore, in the non-adiabatic limit the result of TD-Split of can be viewed as the transfer integral in Marcus theory; when the distortion is weak and the vibrational degrees of freedom do not contribute, TD-Split directly yields the transfer rate.

As a first step towards modeling charge transfer in OPVs, in this paper we use TD-Split in conjunction with time-dependent density functional theory (TDDFT) and time-dependent ZINDO[18] to study electron transfer across a pentacene dimer consisting of two planar stacked pentacene molecules with an intermolecular separation ranging from 3.5 Å to 6.0 Å (see Figure 3.2). The rest of the paper is structured as follows: In Section II we briefly review the approach and discuss computational details, in Section III we present calculations on a pentacene dimer model system, and in Section IV we summarize the results and offer some outlooks on future directions.

3.2 Methodology

3.2.1 Static splitting

In this section, we briefly discuss both the TD-split (dynamic) and static approaches to computing the Marcus coupling term J. In the static picture, one assumes that the charge distribution for the neutral combination is not perturbed (dynamically or statically) by adding an extra electron. If that assumption is correct, the difference in energy between the LUMO+1 and LUMO for the neutral

pair AB is equivalent to the Marcus factor for identical dimers with delocalized orbitals. Transition requires that the LUMO and LUMO+1 are delocalized over both fragments, otherwise the splitting will be high but there will be no transition; this effect is easily included with an additional weight term which measures the delocalization of the LUMO and LUMO+1.

3.2.2 Dynamic splitting

In the dynamic picture (TD-Split), rather than use the LUMO+1 - LUMO of the neutral system to compute the splitting (and thus the charge transfer rate), we instead use the vertical excitation energy (VEE) of the -1 charged dimer from a delocalized ground state, where the extra electron is equally shared between the two fragments. In a Marcus-like picture, this delocalized ground state is akin to an electronic "transition state" for the transferred electron; i.e., the intermediate situation between the charge on one fragment and the charge on the other, and the VEE is thus the electronic coupling between the two diabatic surfaces. Since the nuclear geometries are fixed, this does not correspond to the Marcus intermediate state, but rather to the halfway point in the electron transfer for the given geometry. By using the VEE of the -1 charged dimer from its delocalized ground state, you have carefully chosen the initial and final states in the transfer integral **J** to exclude non-physical re-arrangement of the electrons due to localization on one fragment or the other. In contrast, if you instead compute the transfer starting from a system with the extra electron localized on one fragment you will have added an indeterminate amount of energy; the calculation will thus give non-physical results since the localized charge perturbs the electronic density on the other fragment, and the resulting dynamics from this initial state will be dominated by electronic relaxation rather than transfer. An alternate approach is to use an isolating potential to create initial states with well-defined energies[19]. When the vibrational degrees of freedom are weakly coupled, TD split

corresponds directly to the transfer rate. Note that when the system is not completely symmetric, the rate of transfer can still be obtained using the TD-Split approach from a flux-flux time-dependent calculation which starts with the system in its ground anionic state (delocalized to a certain extent, depending on the degree of asymmetry) and then propagates the fluxes[16]. The flux-flux result is the equivalent of the $|H_{AB}|^2$ term in Marcus theory.

Schematically, the TD- Split approach can be expressed as

$$\delta A \equiv \langle \Psi(t)|A|\Psi(t)\rangle,$$

where $|\Psi(t)\rangle$ is a perturbed ground state for the entire charged system (including donor, acceptor and the extra delocalized electron), and A is the perturbation operator. The time dependent dynamics is thus directly associated with transport since the added charge is delocalized. In this method, the initial state is the ground static density matrix for the entire (donor and acceptor) charged system. A time-dependent excitation is applied and the response to this excitation is a measure of electron transfer rate. As formulated, this method is linear-response in nature. This type of calculation is "dynamic" in the sense that it goes beyond simply using the static eigenvalues of the single-particle Hamiltonian and instead accounts for electronic structure changes during the excitation. For example, in TDDFT this corresponds to correcting the static Kohn-Sham DFT eigenvalue differences with the electron-hole response. As will be shown later, these effects are crucial for properly capturing the separation dependence of the charge transfer.

3.2.3 Computational details

Both the static and dynamic approaches are flexible, as the orbital energies (LUMO, LUMO+1) and the vertical excitation energies can be computed via any number of static and time-dependent

approaches, such as coupled cluster (e.g., equation of motion coupled cluster[20, 21]), linear-response[22, 23] or real-time TDDFT[24-28], or time-dependent semi-empirical methods[18, 29]. In this paper, we use DFT and ZINDO to compute the static splitting and VEEs of a -1 charged pentacene dimer. All DFT/TDDFT calculations were performed with atom-centered Gaussian basis sets using a development version of the NWChem software package[30, 31]. Since these methods are commonplace, we omit the details.

The ZINDO and TD-ZINDO results were obtained by using a modified version of ZINDO-MN package[32]. In a nutshell, in ZINDO only the valence electrons are treated, which is done via semi-empirical one-body (i.e., nuclear and core) parameters h_{ij} and two-body interaction parameters v_{ijkl}, which are fit to experimental data:

$$F_{ij} = h_{ij} + \sum_{kl} v_{ijkl} P_{ij},$$

where P is the density matrix in the atomic orbital basis. The time-dependent response is computed using explicit time propagation via the von Neumann equation:

$$i\frac{\partial P'}{\partial t} = \left[F'\left(P'(t)\right), P'(t)\right],$$

where the prime denotes quantities in the molecular orbital (orthogonal) basis. The actual propagation was carried out using a linear-response von Neumann operator

$$LZ \equiv \frac{dZ}{dt} = -i\frac{[F'(P_0' + \eta Z), P_0' + \eta Z] - [F'(P_0'), P_0']}{\eta}$$

where $Z(t) \equiv P'(t) - P_0'$ is the deviation of the MO density matrix from the initial state, and η is a

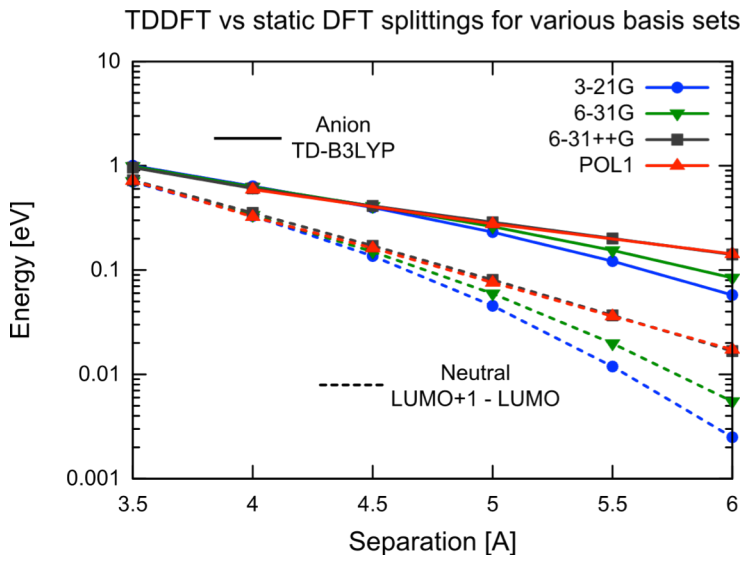

Figure 3.1: Static B3LYP splitting (dashed) and TD-B3LYP energies (solid) for a range of basis sets. Larger separations require a basis set with diffuse functions (e.g., 6-31++G and POL1) to avoid non-physical super-exponential falloff.

small parameter ensuring linearity. $Z(t)$ is propagated from a dipole perturbed ground state $Z_0 = -i[D, P_0']$ via a Chebyshev expansion, and the Fourier transform of the resulting time-dependent dipole moment yields the absorption spectrum, and thus the vertical excitation energies. For all TD-ZINDO simulations, the time step was 0.4 a.u (0.01 fs) and the ZINDO parameters were taken to be as in the original ZINDO-MN package. For a more complete discussion of the TD-ZINDO approach see Ref. [18].

3.3 Results

3.3.1 Convergence with basis set

The large separations in these systems can pose a serious problem for atom-centered basis sets, so as a first step we confirmed that the TDDFT and static splitting (LUMO+1 - LUMO for the neutral dimer) results were all converged with basis.

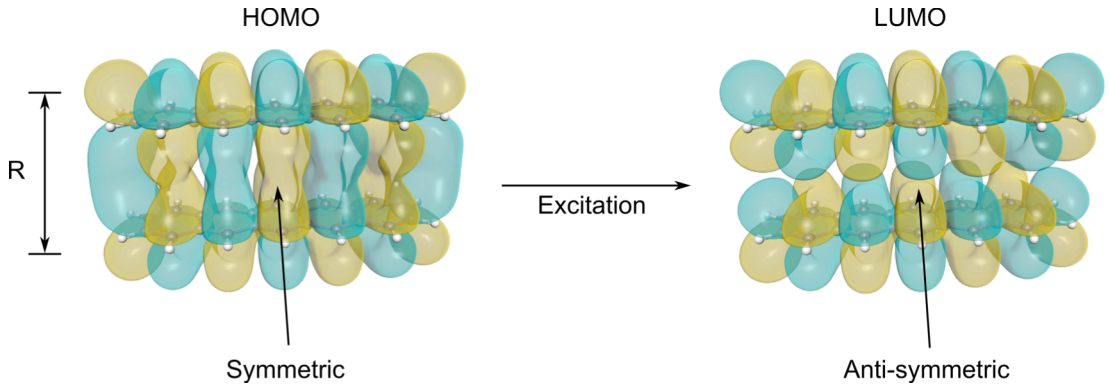

Figure 3.2: Snapshots of the orbitals involved in the vertical excitation of the -1 charged dimer (5 Å separation, PBE, 6-31++G basis). The excitation corresponds to a symmetric → antisymmetric flip of the wavefunction.

Figure 3.1 shows the B3LYP TDDFT vertical excitation energy (VEE) for the negatively charged dimer, and the difference in energy between the LUMO and LUMO+1 for the neutral dimer for the 3-21G, 6-31G, 6-31++G, and POL1 basis sets. For shorter separations (R < 4.5 Å), both the static and TDDFT energies are relatively insensitive to basis set, whereas there is a pronounced deviation from exponential behavior at larger separations for the 3-21G and 6-31G basis sets. The super-exponential falloff (non-linear in log plot) is a non-physical consequence of the insufficient physical extent of the smaller basis sets. The POL1 basis, which is highly diffuse and optimized for response properties, retains the correct exponential falloff, as does the 6-31++G basis, which is a 6-31G basis with extra diffuse functions. The TDDFT VEEs are less sensitive to basis set than the static DFT LUMO+1 – LUMO energies, since individual orbital energies are typically more sensitive to incomplete overlap due to finite basis. Given these results, we henceforth use the 6-31++G basis, which for our purposes yields effectively the same quality results as POL1 with significantly less computational effort (656 basis functions instead of 1308). In general, for calculations of this kind on extended systems, augmenting a small basis with a few diffuse functions offers an affordable way to capture charge transfer processes.

III.2 Static versus dynamic splittings

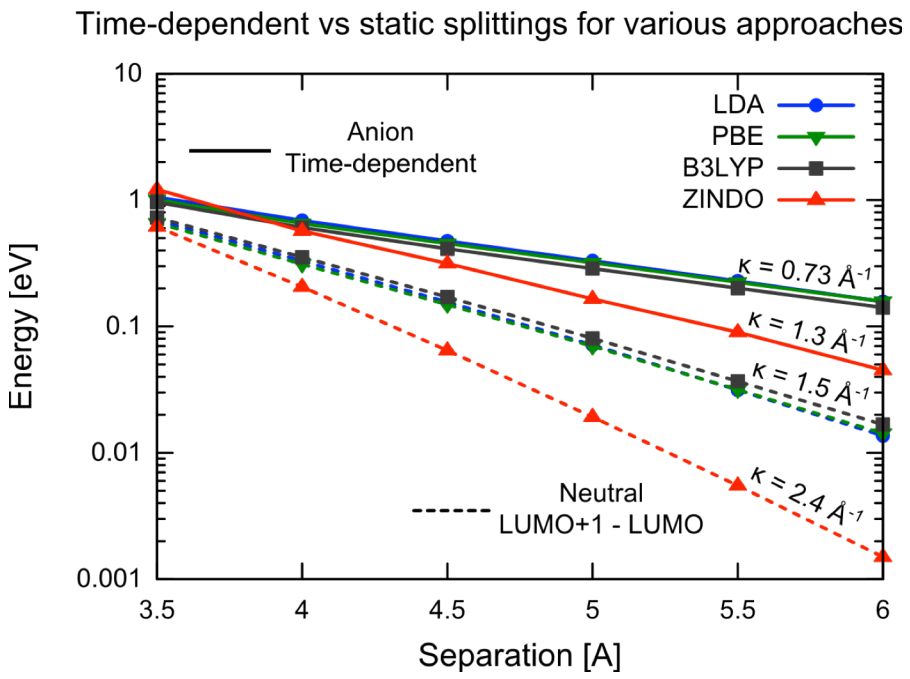

Figure 3.3: Static DFT/ZINDO splitting for the neutral dimer (dashed) and HOMO → LUMO TDDFT/TD-ZINDO vertical excitation energies for the -1 charged dimer (solid); the corresponding exponential decay constants are shown above each curve. All DFT calculations used the 6-31++G basis set. The ZINDO results are scaled by 1.5 for easier comparison.

For the -1 charged system, the HOMO and LUMO are extended across the dimer, and the excitation corresponds to a symmetric → antisymmetric flip for the dimer wavefunction (see Figure 3.2). This is important because transitions between orbitals localized on individual fragments would result in an apparently large splitting, but with no electron transfer. This situation can be remedied somewhat by applying a "delocalizing" potential to the system to force a delocalized initial state but this was unnecessary for this symmetric system. The shapes of the neutral LUMO and LUMO+1 are qualitatively similar to the HOMO and LUMO of the negatively charged dimer (not shown), and since they are likewise extended, the difference in their energy is a fair measure of the static splitting.

Figure 3.3 shows the -1 charged dimer vertical excitation energies using a range of TDDFT exchange-correlation functional: LDA (slater exchange[33] and VWN correlation[34]), PBE[35],

B3LYP[36]. The corresponding DFT neutral dimer LUMO+1 – LUMO energies are shown for comparison. Overall, all TDDFT VEEs are quite insensitive to exchange-correlation functional; B3LYP is slightly red-shifted from LDA and PBE, but all have roughly the falloff rate (exponential decay constant of $\kappa = 0.73\ \text{Å}^{-1}$). For separations less than 4.5 Å, there are intra-fragment excitations which are lower in energy than the HOMO → LUMO excitation. These excitations are independent of separation, however, and with increasing R the HOMO → LUMO transition is guaranteed to become the lowest excitation, since it decays exponentially with separation. The DFT neutral static splittings between the first two virtual states (LUMO+1 vs. LUMO) are likewise insensitive to the functional, but are both significantly shifted lower in energy than the TDDFT VEEs, and also decay much faster ($\kappa = 1.5\ \text{Å}^{-1}$). Figure 3.3 also shows the corresponding static and time-dependent ZINDO results. Since we are interested in the slope rather than absolute energies, they were scaled by 1.5 to facilitate comparison with the DFT results. The ZINDO results are qualitatively similar to DFT, except for steeper exponential falloffs. Better tuning of the ZINDO coupling parameter might lead to better agreement with DFT.

Overall, these results suggest that the neutral static picture drastically underestimates the charge transfer rate, and the underestimation grows rapidly with increased separation. For example, whereas the static PBE energy is only 34% lower than the TD-PBE VEE at 3.5 Å, it is a full order of magnitude smaller at 6 Å. The reason for this is twofold: Firstly, the static picture of orbital energy differences does not include re-arrangement of the electronic density during charge transfer; this is analogous to static DFT orbital energy differences versus TDDFT for traditional excitations. Secondly, the static picture assumes negligible perturbation of the electronic structure of the fragments upon adding an additional electron. Although the qualitative features of the orbitals (e.g., shape and ordering) are qualitatively unchanged by the additional electron, the orbital energetics are

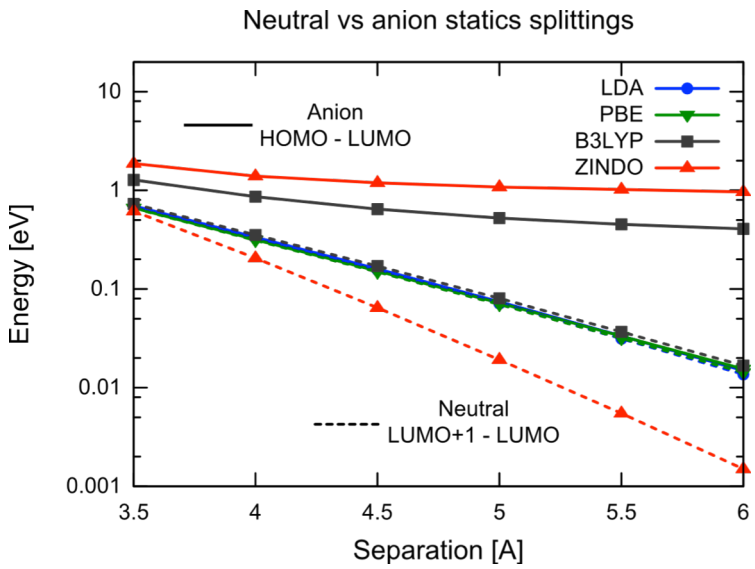

Figure 3.4: Static splitting for the neutral and -1 charged dimer. The two agree well for pure DFT, but the anion is poorly described by B3LYP and ZINDO, due to the failure of HF to capture the delocalized ground state.

affected. For shorter separations, this effect is lessened since the dimer is more like a super-molecule. In a similar vein, the electronic structure of larger systems (e.g., fullerenes) is likewise less sensitive to extra electron.

In devices such as solar cells we are often interested in charge transfer across even larger length scales than these, so it is clear that a time-dependent approach is vital for even a qualitative description of the transfer. For example, it becomes impossible to use a static splitting-based calculation to correlate device morphology with charge transfer, since the static approach predicts far too fast a falloff with separation.

As a final check, we compared the neutral LUMO+1 – LUMO splitting to the -1 charged HOMO – LUMO, as shown in Figure 3.4. For pure DFT functionals (LDA, PBE), the two are virtually identical, which is consistent with the idea that the electronic structure of the dimer is negligibly

affected by the addition of an extra electron. The anion splitting for the hybrid functional (B3LYP), however, is significantly overestimated, and falls off in an incorrect sub-exponential manner. For pure Hartree-Fock (HF; not shown), this is even more pronounced. In a nutshell, HF is driving the system into an ionic-like state rather than a delocalized one, resulting in unphysical orbital energies; this failure of HF to describe anions is well-known. It is not surprising that B3LYP shows this behavior because it contains 20% HF. ZINDO, which is a HF-type method (albeit with modified interaction terms), also suffers from this problem. There are two things to note from these results: First, they confirm that dynamic (time-dependent) effects (e.g., electronic relaxation) are indeed important, and these calculations are not merely a measure of the anion static HOMO – LUMO splitting. Second, even though HF-based methods break down when describing the anionic orbital energies, the corresponding dynamics are still quite reasonable, i.e., the TD-B3LYP excitation energies are in excellent agreement with TD-LDA and TD-PBE, and TD-ZINDO is in reasonable agreement. Put another way, the response of the system is relatively insensitive to the poor ground state description.

3.4 Conclusions

In summary, we computed the electronic couplings for a -1 charged pentacene dimer as a first step towards modeling electron transfer in organic photovoltaics. Two types of splitting were computed: the static DFT and ZINDO LUMO+1 – LUMO of the neutral dimer, and the vertical excitation energy of the -1 charged dimer from a delocalized ground state, which was obtained via time-dependent methods (TDDFT and TD-ZINDO). The static picture consistently underestimates the splitting, and results in a far steeper exponential falloff than the dynamic splitting. As a consequence, while the static splitting offers a decent approximation to the transfer at short

distances, with increasing separation it becomes ever more important to use the dynamic approach. These results have strong implications in systems like organic photovoltaics, where the LUMO+1 - LUMO is a common rule of thumb for estimating charge transfer efficiency, since the addition of an extra electron on a fullerene is usually assumed to not significantly perturb the electronic structure. Care must be taken, however, as using the static approximation for large separations will drastically underestimate transfer probabilities, perhaps even by orders of magnitude in extreme cases. Future studies will address the accuracy of the static versus dynamic picture for charge transfer across fullerene pairs.

Acknowledgments

A portion of the research was performed using the computing resources at EMSL, a national scientific user facility sponsored by the U.S. Department of Energy's (DOE) Office of Biological and Environmental Research and located at Pacific Northwest National Laboratory (PNNL). PNNL is operated for the DOE by the Battelle Memorial Institute under contract DE-AC06-76RLO-1830. The work of R.R, C.A., and D.N. was supported as part of the Molecularly Engineered Energy Materials (MEEM), an Energy Frontier Research Center funded by the U.S. Department of Energy, Office of Science, Office of Basic Energy Sciences under Award Number DE-SC0001342. K.L. acknowledges the William Wiley Postdoctoral Fellowship from EMSL, and N.G. acknowledges the NWChem project for support.

References

[1] K. V. Mikkelsen and M. A. Ratner, "Electron-Tunneling in Solid-State Electron-Transfer Reactions," Chemical Reviews, vol. 87, pp. 113-153, Feb 1987.

[2] W. Zhao, W. H. Ma, C. C. Chen, J. C. Zhao, and Z. G. Shuai, "Efficient degradation of toxic organic pollutants with Ni2O3/TiO2-xBx under visible irradiation," Journal of the American Chemical Society, vol. 126, pp. 4782-4783, Apr 21 2004.

[3] B. Oregan and M. Gratzel, "A Low-Cost, High-Efficiency Solar-Cell Based on Dye-Sensitized Colloidal Tio2 Films," Nature, vol. 353, pp. 737-740, Oct 24 1991.

[4] W. Stier and O. V. Prezhdo, "Nonadiabatic molecular dynamics simulation of light-induced, electron transfer from an anchored molecular electron donor to a semiconductor acceptor," Journal of Physical Chemistry B, vol. 106, pp. 8047-8054, Aug 22 2002.

[5] N. J. Tao, "Electron transport in molecular junctions," Nat Nano, vol. 1, pp. 173-181, 2006.

[6] G. L. Closs and J. R. Miller, "Intramolecular Long-Distance Electron-Transfer in Organic-Molecules," Science, vol. 240, pp. 440-447, Apr 22 1988.

[7] J. L. Bredas, D. Beljonne, V. Coropceanu, and J. Cornil, "Charge-transfer and energy-transfer processes in pi-conjugated oligomers and polymers: A molecular picture," Chemical Reviews, vol. 104, pp. 4971-5003, Nov 2004.

[8] A. Nitzan and M. A. Ratner, "Electron transport in molecular wire junctions," Science, vol. 300, pp. 1384-1389, May 30 2003.

[9] V. Lemaur, D. A. Da Silva Filho, V. Coropceanu, M. Lehmann, Y. Geerts, J. Piris, M. G. Debije, A. M. Van de Craats, K. Senthilkumar, L. D. A. Siebbeles, J. M. Warman, J. L. Bredas, and J. Cornil, "Charge transport properties in discotic liquid crystals: A quantum-chemical insight into structure-property relationships," Journal of the American Chemical Society, vol. 126, pp. 3271-3279, Mar 17 2004.

[10] R. A. Marcus and N. Sutin, "Electron Transfers in Chemistry and Biology," Biochimica Et Biophysica Acta, vol. 811, pp. 265-322, 1985.

[11] Q. Wu and T. Van Voorhis, "Extracting electron transfer coupling elements from constrained density functional theory," Journal of Chemical Physics, vol. 125, Oct 28 2006.

[12] T. Stein, L. Kronik, and R. Baer, "Reliable Prediction of Charge Transfer Excitations in Molecular Complexes Using Time-Dependent Density Functional Theory," Journal of the American Chemical Society, vol. 131, pp. 2818-+, Mar 4 2009.

[13] C. Liu, D. Walter, D. Neuhauser, and R. Baer, "Molecular recognition and conductance in crown ethers," Journal of the American Chemical Society, vol. 125, pp. 13936-13937, Nov 19 2003.

[14] H. N. Chen, M. A. Ratner, and G. C. Schatz, "Time-Dependent Theory of the Rate of Photo-induced Electron Transfer," Journal of Physical Chemistry C, vol. 115, pp. 18810-18821, Sep 29 2011.

[15] C. P. Hsu, "The Electronic Couplings in Electron Transfer and Excitation Energy Transfer," Accounts of Chemical Research, vol. 42, pp. 509-518, Apr 2009.

[16] L. A. Bartell, R. Reslan, M. R. Wall, R. D. Kennedy, and D. Neuhauser, "Electron transfer

with TD-Split, a linear response time-dependent method," Chemical Physics, vol. 391, pp. 62-68, Nov 24 2011.

[17] R. J. Cave and M. D. Newton, "Generalization of the Mulliken-Hush treatment for the calculation of electron transfer matrix elements," Chemical Physics Letters, vol. 249, pp. 15-19, Jan 26 1996.

[18] L. A. Bartell, M. R. Wall, and D. Neuhauser, "A time-dependent semiempirical approach to determining excited states," Journal of Chemical Physics, vol. 132, Jun 21 2010.

[19] H. Eshuis and T. van Voorhis, "The influence of initial conditions on charge transfer dynamics," Physical Chemistry Chemical Physics, vol. 11, pp. 10293-10298, 2009.

[20] R. J. Bartlett and M. Musial, "Coupled-cluster theory in quantum chemistry," Reviews of Modern Physics, vol. 79, pp. 291-352, Jan-Mar 2007.

[21] K. Kowalski and P. Piecuch, "New coupled-cluster methods with singles, doubles, and noniterative triples for high accuracy calculations of excited electronic states," Journal of Chemical Physics, vol. 120, pp. 1715-1738, Jan 22 2004.

[22] M. E. Casida, in Recent Advances in Density Functional Methods. vol. 1, D. P. Chong, Ed., ed River Edge, NJ: World Scientific Publishing, 1995, pp. 155-192.

[23] S. Hirata and M. Head-Gordon, "Time-dependent density functional theory for radicals - An improved description of excited states with substantial double excitation character," Chemical Physics Letters, vol. 302, pp. 375-382, Mar 26 1999.

[24] C. L. Moss, C. M. Isborn, and X. S. Li, "Ehrenfest dynamics with a time-dependent density-

functional-theory calculation of lifetimes and resonant widths of charge-transfer states of Li(+) near an aluminum cluster surface," Physical Review A, vol. 80, Aug 2009.

[25] K. Yabana and G. F. Bertsch, "Time-dependent local-density approximation in real time," Physical Review B, vol. 54, pp. 4484-4487, Aug 15 1996.

[26] A. Castro, H. Appel, M. Oliveira, C. A. Rozzi, X. Andrade, F. Lorenzen, M. A. L. Marques, E. K. U. Gross, and A. Rubio, "octopus: a tool for the application of time-dependent density functional theory," Physica Status Solidi B-Basic Solid State Physics, vol. 243, pp. 2465-2488, Sep 2006.

[27] K. Lopata and N. Govind, "Modeling Fast Electron Dynamics with Real-Time Time-Dependent Density Functional Theory: Application to Small Molecules and Chromophores," Journal of Chemical Theory and Computation, vol. 7, pp. 1344-1355, May 2011.

[28] R. Baer and D. Neuhauser, "Real-time linear response for time-dependent density-functional theory," Journal of Chemical Physics, vol. 121, pp. 9803-9807, Nov 22 2004.

[29] J. D. Baker and M. C. Zerner, "Applications of the Random Phase Approximation with the Indo/S Hamiltonian - Uv-Vis Spectra of Free Base Porphin," Chemical Physics Letters, vol. 175, pp. 192-196, Dec 7 1990.

[30] M. Valiev, E. J. Bylaska, N. Govind, K. Kowalski, T. P. Straatsma, H. J. J. Van Dam, D. Wang, J. Nieplocha, E. Apra, T. L. Windus, and W. de Jong, "NWChem: A comprehensive and scalable open-source solution for large scale molecular simulations," Computer Physics Communications, vol. 181, pp. 1477-1489, Sep 2010.

[31] NWChem. Available: http://www.nwchem-sw.org/

[32] M. C. Zerner, "ZINDO-MN," Version 2011 ed: Quantum Theory Project, University of Florida, Gainesville, FL; Department of Chemistry, University of Minnesota, Minneapolis, MN, 2011.

[33] J. C. Slater and K. H. Johnson, "Self-Consistent-Field Chi Alpha Cluster Method for Polyatomic-Molecules and Solids," Physical Review B, vol. 5, pp. 844-&, 1972.

[34] S. H. Vosko, L. Wilk, and M. Nusair, "Accurate Spin-Dependent Electron Liquid Correlation Energies for Local Spin-Density Calculations - a Critical Analysis," Canadian Journal of Physics, vol. 58, pp. 1200-1211, 1980.

[35] J. P. Perdew, K. Burke, and M. Ernzerhof, "Generalized gradient approximation made simple (vol 77, pg 3865, 1996)," Physical Review Letters, vol. 78, pp. 1396-1396, Feb 17 1997.

[36] P. J. Stephens, F. J. Devlin, C. F. Chabalowski, and M. J. Frisch, "Ab-Initio Calculation of Vibrational Absorption and Circular-Dichroism Spectra Using Density-Functional Force-Fields," Journal of Physical Chemistry, vol. 98, pp. 11623-11627, Nov 10 1994.

Chapter 4

Excited-State Studies of Polyacenes: A Comparative Picture Using EOMCCSD, CR-EOMCCSD(T), Range-Separated (LR/RT)-TDDFT, TD-PM3 and TD-ZINDO

The low-lying excited states (L_a and L_b) of polyacene from naphthalene to heptacene (N=2-7) are studied using various time-dependent computational approaches. We perform high-level excited-state calculations using equation of motion coupled cluster with singles and doubles (EOMCCSD) and completely renormalized equation of motion coupled cluster with singles, doubles, and perturbative triples (CR-EOMCCSD(T)) and use these results to evaluate the performance of various range-separated exchange-correlation functionals within linear-response (LR) and real-time (RT) time-dependent density functional theories (TDDFT). As has been reported recently, we find that the range-separated family of functionals addresses the well-documented TDDFT failures in describing these low-lying singlet excited states to a large extent and are as about as accurate as results from EOMCCSD on average. Real-time TDDFT visualization shows that the excited state charged densities are consistent with the predictions of the perimeter free electron orbital (PFEO) model. This corresponds to particle-on-ring confinement, which leads to the well-known red-shift of the excitations with acene length. We also use time-dependent semi-empirical methods like TD-

PM3 and TD-ZINDO, which are capable of handling very large systems. Once re-parameterized to match the CR-EOMCCSD(T) results, TD-ZINDO becomes roughly as accurate as range-separated TDDFT, which opens the door to modeling systems such as large molecular assemblies.

4.1 Introduction

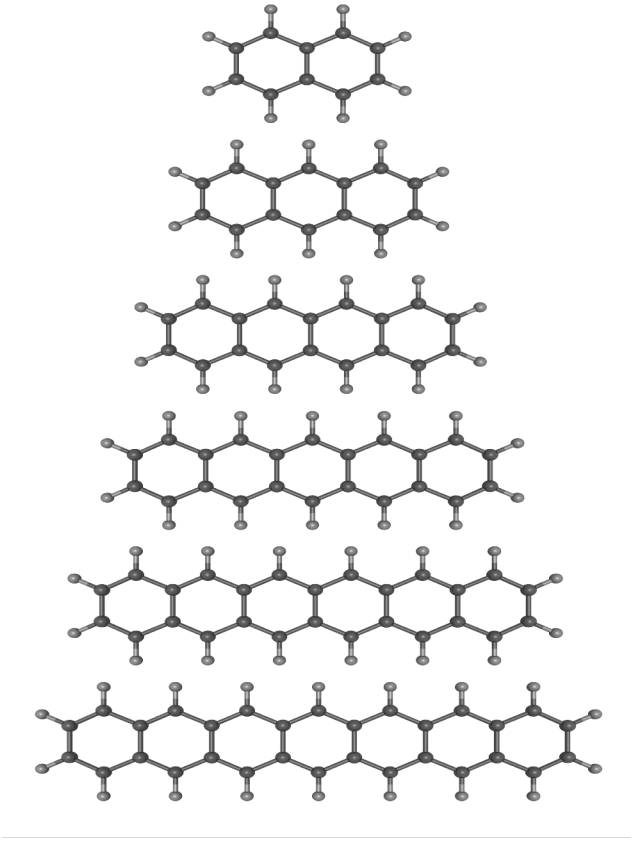

Figure 4.1 Structures of the acenes studied. From top to bottom: naphthalene (N=2), anthracene (N=3), tetracene (N=4), pentacene (N=5), hexacene (N=6), heptacene (N=7)

Polyacenes or acenes constitute a class of polycyclic organic compounds consisting of linearly fused benzene rings. These compounds, and their derivatives, have been studied extensively and over the last several years the larger representatives in this class have been used in a plethora of applications such as light-emitting diodes,[1-4] photovoltaic cells,[5-7] liquid crystal displays,[8] organic field-effect transistors[9,10] to name a few. Pentacene, in particular, has received much attention because of its high charge-carrier (hole) mobility in films and molecular crystals.[11-13] For an overview of the electronic applications of acenes, see the reviews by Anthony.[14,15]

In a nutshell, the electronic properties of these materials are dictated by the π electrons which occupy the highest occupied and lowest unoccupied states; the π interactions between adjacent

acene molecules, for example, gives rise to the high hole mobility through molecular films. In a single molecule, the lowest valence excitations have $\pi - \pi^*$ character and the two lowest singlet excitations are commonly assigned as the L_a (B_{2u} symmetry) and L_b (B_{3u} symmetry) states, respectively. The former represents the polarization along the short-axis, whilst the latter represents the polarization along the long-axis. The L_b is the lowest excited-state in benzene and naphthalene but switches positions with the L_a state for larger acenes, with the crossing happening around anthracene. It has long been suggested, from a valence-bond point of view, that the L_a state is mostly ionic in character involving significant rearrangement of the excited-state density, whereas the L_b state is mostly covalent where the excited-state density is similar to the ground state.

There has been significant progress in describing these excitations theoretically,[16-23] within which time-dependent density functional theory (TDDFT)[24-26] has been the predominant method. It is now well-known, however, that for TDDFT traditional and global hybrid functionals fail to describe these lowest excitations. Grimme and Parac demonstrated that the ordering switches earlier than expected with both classes of functionals and the excitation energy of the L_a state is severely underestimated and progressively worsens with system size.[20] Increasing the Hartree-Fock (HF) content in the exchange-correlation improves the picture for the L_a but worsens the excitation energy of the L_b state. They concluded that it was impossible to capture both states accurately just by adjusting the HF content.

Very recently, range-separated hybrid (RSH) functionals have been applied to the L_a state in acenes.[17-19, 22] RSHs correct the incorrect asymptotic behavior of the exchange by splitting the exchange into a short-range part and long-range part. For many optically active charge transfer states, RSHs rival the accuracy of the equation of motion coupled cluster singles doubles (EOMCCSD) method on average. The success of RSHs in this case, however, is in many ways quite

surprising, as the L_a state is an intra-molecular transverse excitation (along short-axis of molecule) and clearly not long-range at all. Richard and Herbert labeled this a charge-transfer-like state in disguise,[18] which Kuritz et al. subsequently rationalized as arising from minimal overlap in auxiliary orbitals,[19] akin to minimal overlap of the hole/charge orbitals in a typical charge transfer excitation.

In some sense, acenes serve as a rough prototype for more complicated light harvesting system, and also as the fundamental building block for many molecular electronic devices. Careful analysis of the excitations in these deceptively simple molecules serves as a crucial test for the accuracy and predictive power of a theoretical technique, as indicated by the intense interest in benchmarking TDDFT results in these systems. In this light, our main goal in this paper is to examine the low-lying excited states of polyacenes from naphthalene to heptacene (Figure 4.1) using a wide selection of time-dependent approaches. We first perform a systematic analysis based on high-level coupled cluster (EOMCCSD and CR-EOMCCSD(T)) calculations. These calculations are used to benchmark the performance of various range-separated exchange-correlation functionals implemented within linear response and real-time TDDFT. Additionally, we explore the use of semi-empirical time-dependent PM3 and ZINDO for describing these excitations, and reparametrize their Hamiltonians to better match the results of high level theory. All structures were obtained using cc-pVTZ/B3LYP.

The rest of the paper is organized as follows: In section 4.2, we briefly review the various time-dependent approaches used in this study and provide the necessary computational details. The results are presented and discussed in section 4.3 and the concluding remarks in section 4.4.

4.2 Methodologies and computational details

Below we briefly review the formalisms for equation of motion coupled cluster (EOMCC), real-time time-dependent density functional theory (RT-TDDFT), and real-time time-dependent PM3 and

ZINDO. All results except the PM3 and ZINDO ones were obtained using NWChem.[27] The TD-PM3 results were obtained by a modification of the PM3 module from MOPAC 6.0,[28,29] to perform iterative time-dependent calculation of the TD-PM3 excitation energies.[30] The TD-ZINDO results were obtained by an analogous modification of ZINDO from the ZINDO-MN package.[31] The linear response TDDFT results were calculated using the module in NWChem; since the approach is widely used (e.g., refs 26 and 32), we omit the details.

4.2.1 Equation of motion coupled cluster

The EOMCC formalism[33] can be viewed as an excited-state extension of single-reference coupled cluster method, where the wavefunction corresponding to the K-th state is represented as

$$|\Psi_K\rangle = R_K e^T |\Phi\rangle \tag{4.1}$$

where T and state-specific R_K operators are the cluster and excitation operators, respectively, and $|\Phi\rangle$ is the so-called reference function usually chosen as a Hartree-Fock determinant. Various approximate schemes range from the basic EOMCCSD approximation where the cluster and correlation operators are represented as sums of scalar ($R_{K,0}$ for excitation operator only), single ($T_1, R_{K,1}$) and double ($T_2, R_{K,2}$) excitations

$$|\Psi_K^{EOMCCSD}\rangle = (R_{K,0} + R_{K,1} + R_{K,2}) e^{T_1+T_2} |\Phi\rangle \tag{4.2}$$

to the more advanced EOMCCSDT and EOMCCSDTQ approach, accounting for the effect of triple and/or quadruple excitations. It has been demonstrated that the progression of methods: EOMCCSD ⟶ EOMCCSDT ⟶ EOMCCSDTQ..., in the limit converge to the exact (full configuration interaction) energies. However, the rapid growth in the numerical complexity of the

EOMCC methods makes calculations with the EOMCCSDT or EOMCCSDTQ methods very expensive even for relatively small systems. Unfortunately, the EOMCCSD method is capable of providing reliable results only for singly excitedstates. However, as it has recently been demonstrated,[34] errors in the range of 0.25-0.30 eV with respect to the experimental vertical excitation energies (VEE) persist with increasing system size.

In order to narrow the gap between the EOMCCSD and EOMCCSDT VEEs, several non-iterative N^7-scaling methods that mimic the effect of triples in a perturbative fashion have been proposed in the past.[35-40] The completely renormalized EOMCCSD(T) approach, denoted CR-EOMCCSD(T),[41] falls into this class (see also refs 42 and 43-45 for the most recent developments). In this approach the energy correction $\delta_K^{CR-EOMCCSD(T)}$ is added

to the EOMCCSD VEE ($\omega_K^{EOMCCSD}$)

$$\omega_K^{CR-EOMCCSD(T)} = \omega_K^{EOMCCSD} + \delta_K^{CR-EOMCCSD(T)} \tag{4.3}$$

where the $\delta_K^{CR-EOMCCSD(T)}$ is expressed through the trial wavefunction $\langle \Psi_K |$ and the triply excited EOMCCSDmoment operator $M_{K,3}^{EOMCCSD}$ (see ref 41 for details):

$$\delta_K^{CR-EOMCCSD(T)} = \frac{\left\langle \Psi_K \middle| M_{K,3}^{EOMCCSD} \middle| \Phi \right\rangle}{\left\langle \Psi_K \middle| (R_{K,0} + R_{K,1} + R_{K,2}) e^{T_1+T_2} \middle| \Phi \right\rangle} \tag{4.4}$$

Although the CR-EOMCCSD(T) method is characterized by the same N^7 scaling as the ground-state CCSD(T) method\cite{raghavachari_1989_ccsd_t}, the fact that triply excited EOMCCSD moments needs to be calculated makes this approach few times more expensive than the ground-state CCSD(T) approach.

4.2.2 Real-time TDDFT

In real-time time-dependent density functional theory (RT-TDDFT), the time-dependent Kohn-Sham (KS) equations are explicitly propagated in time:

$$i\frac{\partial\psi_i(r,t)}{\partial t} = [-\frac{1}{2}\nabla^2 + v_{KS}[\rho](r,t)]\psi_i(t) \tag{4.5}$$

$$= \left[-\frac{1}{2}\nabla^2 + v_{ext}(r,t) + v_H(r,t) + v_{XC}[\rho](r,t)\right]\psi_i(t) \tag{4.6}$$

where $\rho(r,t)$ is the charge density, $v_{ext}(r,t)$ is the external potential describing the nuclear-electron and applied field contributions, $v_H(r,t)$ is the electron-electron potential, and $v_{XC}[\rho](r,t)$ is the exchange-correlation potential, which is henceforth assumed to depend only on the instantaneous density (adiabatic approximation). In a Gaussian-orbital basis it is simpler to work with density matrices rather than KS orbitals, in which case the evolution of the electronic density is governed by the von Neumann equation:

$$i\frac{\partial P'}{\partial t} = [F'(t), P'(t)] \tag{4.7}$$

where the prime notation denotes matrices in the orthogonal molecular orbital (MO) basis, and unprimed denotes matrices in the atomic orbital (AO) basis. Note that in eq 4.7, all matrices are complex quantities. The Fock matrix $F(t)$ is computed in the AO basis similar to ground state DFT, with the important distinction that in the absence of Hartree-Fock exchange (e.g., pure DFT), $F(t)$ is real symmetric and only depends on the real part of $P(t)$. If HF exchange is included (e.g, hybrid functionals), it becomes complex Hermitian (see ref 47 for details of the NWChem RT-TDDFT implementation, derivations, and references).

There are numerous approaches taken to propagating eq 4.7. In this study, we use a second order Magnus scheme, which is equivalent to an exponential midpoint propagator

$$P'(t+\Delta t) = e^{-iF'(t+\Delta t/2)\Delta t} P'(t) e^{iF'(t+\Delta t/2)\Delta t} \quad (4.8)$$

where we compute the Fock matrix at the future time via linear extrapolation from the previous two values, followed by iterative interpolation until converged. This approach is extremely stable, as it maintains the idempotency of the density matrix, and yields order $(\Delta t)^2$ accuracy. In practice, this allows for time steps on the order of $\Delta t = 0.1\ \text{au} = 2.42 \times 10^{-3}\ fs$ with minimal loss of accuracy. The exponentiation of eq 4.8 is done via contractive power series, where the operator is first divided by 2^m such that the norm of the scaled operator is less than 1, performing the power series (which is guaranteed to converge well numerically since it is contractive), then squaring the result m times to recover the result. All real-time TDDFT simulations here used a time step of $\Delta t = 0.2\ \text{au} = 0.0048\ fs$ and ran up to $1500\ au = 36.3\ fs$, which corresponds to 7500~time steps.

To obtain spectroscopic information, the system is excited via a linearly polarized (x, y, z) narrow Gaussian electric field kick which adds to the Fock matrix via dipole coupling:

$$E(t) = \kappa exp[-(t-t_0)^2/2w^2]\hat{d} \quad (4.9)$$

where $\hat{d} = \hat{x}, \hat{y}, \hat{z}$ is the polarization, κ is the field maximum (dimensions of electric field), t_0 is the center of the pulse, and w is the width, which is typically~ Δt. This induces all electronic modes simultaneously, and the Fourier transform of the resulting time-dependent dipole moment yields the absorption spectrum for that polarization; the sum of the three spectra gives the full absorption. In the limit of a small electric field perturbation, real-time TDDFT and linear-response yield essentially identical spectroscopic results; unlike LR-TDDFT, RT-TDDFT is also valid in the strong perturbation regime, but the studies presented here are all the weak-field and thus comparable to

LR-TDDFT. All kick-type results here used a kick with $\kappa = 0.002\ au = \frac{1.0V}{nm}, t_0 = 3.0\ au = 0.07\ fs, and\ w = 0.2\ au = 0.0048\ fs$

The true power of RT-TDDFT, however, lies in direct modeling of the electron dynamics in response to a realistic stimulus, such as a laser tuned to resonance with a particular electronic transition. For example, to excite the system into a particular state of interest, it is simplest to use a Gaussian enveloped monochromatic laser pulse of the form:

$$E(t) = \kappa exp\left[-\frac{(t-t_0)^2}{2w^2}\right]\cos(\omega_0 t)\hat{d} \tag{4.10}$$

where ω_0 is the driving frequency, and w is broad enough to encapsulate at least a few oscillations. In this case, the charge density can be visualized in 4D (three space + time) which yields detailed insight into the fundamental nature of the excitation. This is especially important as an intuitive metric for characterizing charge transfer excitations, and when elucidating the mechanism of excitations. In this paper, RT-TDDFT is used as a visual tool to assign longitudinal and transverse excitations into two distinct classes (ionic vs covalent, respectively), and to study the physical origin of the red-shift with acene length.

4.2.3 Time-dependent semi-empirical methods

A well known alternative to first-principles approaches is semi-empirical methods (e.g., PM3[28] and ZINDO[48]) which can be extended to a time-dependent formalism.[30] A minimal valence basis set is used, so that there are only 4 orbitals for each carbonatom. Typically, the Fock matrix has the generic Hartree-Fock-like form:

$$F_{ij} = h_{ij} + \sum_{kl} v_{ijk} P_{ij} \tag{4.11}$$

where h_{ij} and v_{ijk} are semi-empirical one-body and interaction parameters, respectively. Unlike Hartree-Fock and DFT, however, the interaction parameters are restricted to be at most two-center. The calculations are done in an atomic basis (rather than molecular orbital basis, which earlier TD-semi-empirical methods use) so that the calculation of the Fock matrix scales like N^2, where N is the number of orbitals.

After the initial SCF solution labeled as P_0, the same von Neumann equation as in TDDFT (eq 4.7) is propagated. While the same real-time approach as in eq 4.8 could have been used, here however a different algorithm is found to be more efficient. The algorithm has been covered recently (see ref 30), so it will only be briefly reviewed. Basically, the linear-response von Neumann operator is constructed:

$$LZ \equiv \frac{dZ}{dt} = -i\frac{[F(P_0 + \eta Z), P_0 + \eta Z] - [F(P_0), P_0]}{\eta} \tag{4.12}$$

for the deviation from the initial density matrix:

$$Z \equiv P - P_0 \tag{4.13}$$

and η is a small parameter ensuring linearity. Then, the time-dependent dynamics are represented by writing a Chebyshev algorithm for the propagator:

$$Z(t) = e^{Lt}Z_0 = \sum_n (2 - \delta_{n0}) J_n(t\Delta H) T_n(\frac{L}{\Delta H}) Z_0 \tag{4.14}$$

where we introduced the Bessel and modified Chebyshev operators, with the latter propagated as:

$$T_n(\frac{L}{\Delta H})Z_0 = 2\frac{L}{\Delta H}T_{n-1}\left(\frac{L}{\Delta H}\right)Z_0 + T_{n-2}(\frac{L}{\Delta H})Z_0 \tag{4.15}$$

and

$$Z_0 = -i\,[D, P_0] \tag{4.16}$$

where D is the dipole moment matrix. ΔH is half the spectrum width, so that $(\Delta H)^{-1}$ is the effective time-step; it is quite large (almost 0.4~a.u.), so that the overall number of iterations required is quite small (a few thousands even without any signal processing approaches). This approach minimizes the number of matrix multiplications, which in semi-empirical calculations are the most time-consuming steps (scales as N^3 unless sparse matrix algorithms are used). Further savings are obtained by Fourier transforming the time-dependent Bessel function coefficients in eq 4.14 analytically, thereby reducing the required number of iterations. As with RT-TDDFT, spectroscopic information is obtained via kick-type excitations.

4.3 Results

In this section we present acene vertical excitation energies (VEEs) for a wide range of theories: Coupled cluster (EOMCCSD, CR-EOMCCSD(T)); linear response TDDFT with a global hybrid functional (B3LYP[49]) and a variety of range-separated functionals (CAM-B3LYP,[50] LC-BLYP, LC-ωPBE,[51] BNL[52]) real-time TDDFT with the BNL functional; and two semi-empirical methods (TD-ZINDO, TD-PM3). Before discussing results, it is important to note that vertical excitation energies, which correspond to the energy difference between ground and excited states without a change in geometry, cannot be directly measured experimentally (see ref 21). As a good approximation, VEEs can be measured experimentally via the locations of experimental UV-Vis absorption peaks, but the accuracy of this approximation varies depending on state and molecule, with deviations typically on the order of a few tenths of an eV. To ensure meaningful comparisons between the computed VEEs and experimental results, we use the corrected acene experimental values from Grimme and Parac[20] (see ref 53 for the original experimental results). In a nutshell,

these incorporate adjustments to the L_a and L_b computed from TDDFT (B3LYP/TZVP) excitation energies with fully optimized excited state geometries (calculated for acenes $\mathrm{N} = 2, 3, 4$; extrapolated to N=5, 6, 7). This somewhat accounts for geometry relaxation effects, but significant theory-experiment discrepancies still arise from basis set quality and the level of theory, specifically the treatment of correlation effects.

The L_a and L_b vertical excitation energies for the set of acenes are summarized in Table 4.1, along with the corrected experimental values, and the mean average error (MAE) from experiment, for the full set of acenes for each approach. These VEEs (for a few representative theories) are plotted against acene size in Figure 4.4. Qualitatively speaking, all methods capture most of the gross features, including red-shift of the L_b (longitudinal) state with acene length, and steeper red-shift of the L_a (transverse) state with acene length. However, there is only mixed success in describing the important experimentally observed crossover of lowest energy state from $L_a \rightarrow L_b$ around anthracene; this is discussed in more detail below.

4.3.1 Equation-of-motion coupled cluster

Overall, CR-EOMCCSD(T) has the best agreement with experimental energies, with a MAE of 0.07~eV for the L_a state, and 0.06~eV for the L_b. Most importantly, CR-EOMCCSD(T) simultaneously describes both states well, and captures the crossover at the right energy (near anthracene). That is, it predicts that L_a is lower in energy than L_b for naphthalene, they are roughly equal for anthracene, and L_b is lower afterwords (see Figure 4.2). In contrast to the experimental vertical excitation energies, the EOMCCSD and CR-EOMCCSD(T) approaches predict for anthracene the reversed ordering of the L_a and L_b states. The CR-EOMCCSD(T) excitation energy for L_b state is located 0.1 eV below the one corresponding to the L_a state. Similar reverse ordering

has been reported in the context of multireference Møller-Plesset (MRPT) theory[54,55] calculations for low-lying excited states of anthracene.[16] In the case of the MRPT approach, the 0.17 eV separation between L_b and L_a states is slightly larger than 0.1 eV obtained with the CR-EOMCCSD(T) method for POL1 basis set. The CC2 model,[56] which is an approximation to the EOMCCSD formalism, predicts the L_a state to the lowest state, and the calculated separation between L_a and L_b states is around 0.2 eV.

4.3.2 Linear response TDDFT

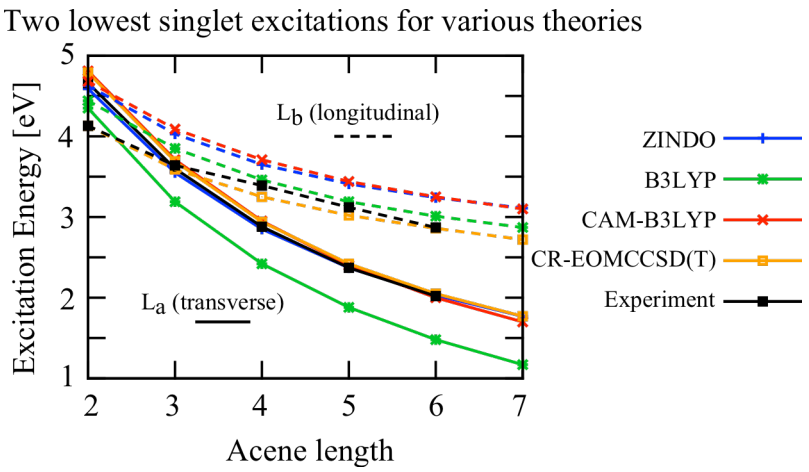

Figure 4.2 Comparison between the two lowest singlet excitation energies of the set of acenes for a selection of theories, along with the experimental values. The solid lines correspond to the L_a (transverse) excitation, and the dashed lines to the L_b (longitudinal) excitation.

The range-separation parameter for the CAM-B3LYP,[50] LC-BLYP and BNL[52] functionals was taken to be $0.33\ au^{-1}$; for LC-ωPBE,[51] it was $0.30\ au^{-1}$. For the transverse charge-transfer-like L_a state (solid lines in Figure 4.2), all the range-separated TDDFT results agree well with experiment and EOMCC, with MAE typically around a few hundredths of an eV. Real-time BNL results are essentially the same as the corresponding linear response ones, since the kick perturbation was small. Range-corrected TDDFT is less accurate for the L_b state, however, with MAEs of $\sim 0.3\ eV$, which is almost twice that of B3LYP. Thus, range-separated TDDFT excels at predicting the challenging charge-transfer-like L_a state, but using a range-

separated functional significantly compromises the accuracy of the L_b state versus a global hybrid approach (e.g., B3LYP). To better understand the accuracy of RSH functionals, two versions of the CAM-B3LYP functional were studied: The first, denoted ``CAM-B3LYP(I)" has an asymptote of $0.65/r$ (i.e., $\alpha + \beta = 0.65$ while the second, denoted ``CAM-B3LYP (II)" has an asymptote of $1.0/r$. The full Hartree-Fock asymptote in the exchange in CAM-B3LYP(II) improves the accuracy in the L_a state at a cost of slightly decreasing the accuracy of the L_b state. On another note, range-separated TDDFT correctly predicts the $L_a \rightarrow L_b$ crossover (intersection of like colored solid and dashed lines in Figure 4.2), albeit at a lower energy than experiment. B3LYP, in contrast, fails to even qualitatively capture this crossover. In short, using range-separated functionals overcomes many of the failures of pure or hybrid DFT functionals in describing the transverse L_a state and the $L_a \rightarrow L_b$ crossover, with overall accuracy rivaling that of CC2. The use of "tuned" RSHs, which has been pioneered by Baer and coworkers,[57] shows promise in further improving the accuracy of TDDFT for systems such as this.[19]

4.3.3 Time-dependent PM3 and ZINDO

We performed time-dependent simulations with two typical semiempirical methods, PM3 and ZINDO. The latter is well known to be better for spectra, as our results indicate. In order to parametrize the TD-ZINDO approach against the coupled CR-EOMCCSD(T) results for the charge-transfer-like L_a, we scaled down the strength of the $\pi\pi'$ interaction potentials, as is commonly done in ZINDO. We found a scaling factor of 0.64, which we denote "ZINDO (II)", yielded the best fit, compared to the stockscaling factor of 0.70 (denoted "ZINDO (I)"). In the case of the general ZINDO (I), the L_a is fairly poorly described (MAE of 0.24~eV) whereas the longitudinal L_b is quite well described, akin to the B3LYP results. The L_a-tuned ZINDO(II),

however, is extremely accurate for the L_a state, but as with range-separated TDDFT, the corresponding accuracy in the L_b state suffers. One drawback of ZINDO, however, is that it fails to properly capture the crossover. ZINDO (I) predicts that L_a and L_b are roughly equal in energy at $N = 2$, whereas ZINDO (II) incorrectly predicts that L_b is always higher in energy than L_a. Of course, the excellent quality of ZINDO (II) results for the L_a. are a consequence of being fit to this particular state, but it is still quite remarkable that with a single parameter it is possible to simultaneous fit six molecules so well. These results suggest carefully parametrized semi-empirical approaches are an excellent tool for modeling excitations in large polyaromatichydrocarbons, where large system size makes coupled cluster, or even TDDFT, unfeasible.

4.3.4 Real-time visualization of the excited charge density

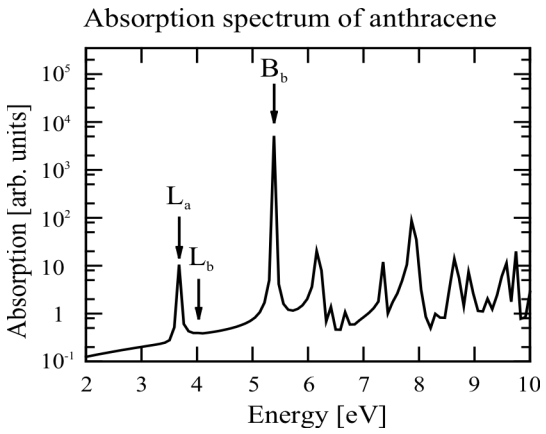

Figure 4.3 Absorption spectrum of anthracene (N=3) obtained via RT-TDDFT (POL1/BNL). The bright L_a and dim L_b peaks correspond to transverse and longitudinal excitations,respectively. The intensely bright longitudinal UV B_b peak is visualized in Figure 4.4 but not compared in Table 4.1

Next, to gain insight into the nature of the excitations we present real-time real-space visualization of the excited state charge density for the (transverse) L_a state. The (longitudinal) L_b state has too small an oscillator strength to visualize clearly, so the major bright longitudinal UV B_b absorption (see Figure 4.3) was chosen as an illustrative analogue (note this peak is not compared in Table 4.1). As before, the system was described using the BNL functional, and for speed the smaller 6-31G** basis set was used instead of POL1. The spectra of the acenes with 6-31G** basis sets were extremely similar to the POL1 spectra, save a slight blue-shift due to the smaller basis.

N	PM3	ZINDO (I)	ZINDO (II)	B3LYP	CAM-B3LYP (I)	CAM-B3LYP (II)	LC-BLYP	LC-ωPBE	BNL	BNL (real-time)	CC2[20]	EOM-CCSD	CR-EOM-CCSD(T)	exptl[20]
							L_a state (transverse; bright)							
2	3.50	4.23	4.59	4.35	4.64	4.81	4.77	4.77	4.86	4.79	4.88	5.09	4.79	4.66
3	2.94	3.30	3.55	3.19	3.51	3.71	3.66	3.66	3.72	3.68	3.69	4.00	3.69	3.60
4	2.53	2.67	2.85	2.42	2.75	2.95	2.91	2.90	2.94	2.91	2.90	3.25	2.94	2.88
5	2.22	2.23	2.37	1.88	2.21	2.40	2.37	2.37	2.39	2.41	2.35	2.72	2.42	2.37
6	1.99	1.92	2.03	1.48	1.82	2.00	1.99	1.99	2.00	1.96	1.95	2.34	2.05	2.02
7	1.81	1.68	1.77	1.17	1.52	1.70	1.69	1.70	1.70	1.69	1.60	2.05	1.77	–
MAE	0.47	0.24	0.03	0.44	0.12	0.08	0.05	0.04	0.08	0.07	0.08	0.37	0.07	–
XAE	1.16	0.43	0.07	0.54	0.20	0.15	0.11	0.11	0.20	0.13	0.22	0.43	0.13	–
							L_b state (longitudinal; dim)							
2	3.34	4.21	4.63	4.44	4.59	4.68	4.58	4.58	4.64	4.61	4.46	4.43	4.13	4.13
3	2.91	3.67	4.03	3.85	4.02	4.09	4.02	4.02	4.07	4.03	3.89	3.90	3.59	3.64
4	2.62	3.32	3.65	3.46	3.64	3.71	3.65	3.65	3.70	3.68	3.52	3.54	3.25	3.39
5	2.42	3.10	3.41	3.19	3.38	3.44	3.39	3.40	3.44	3.42	3.27	3.30	3.02	3.12
6	2.27	2.96	3.24	3.01	3.20	3.25	3.21	3.22	3.26	3.23	3.09	3.12	2.86	2.87
7	2.15	2.82	3.11	2.87	3.06	3.10	3.07	3.09	3.12	3.03	2.97	2.99	2.74	–
MAE	0.72	0.06	0.36	0.16	0.34	0.40	0.34	0.34	0.39	0.36	0.22	0.23	0.06	–
XAE	0.79	0.09	0.50	0.31	0.46	0.55	0.45	0.45	0.51	0.48	0.33	0.30	0.14	–

[a] The L_a state corresponds to a transverse excitation with high oscillator strength (bright) and the L_b state to a longitudinal excitation with low oscillator strength (dim). All TDDFT results are linear response unless noted otherwise.

Table 4.1 The two lowest excitation energies in eV for the N=2-7 series of acenes for a range of theories, and the corresponding mean absolute error (MAE) and maximum absolute error (XAE) in eV from the experimental values.

Figure 4.4 shows real-time TDDFT snapshots of the deviation of the charge density from the ground state for anthracene and heptacene after resonant excitation to the L_a state. Unlike plots of molecular orbitals, which are strictly ground state quantities, Figure 4.4 corresponds to the actual charge density dynamics resulting from an excitation. For the longitudinal excitation (top), blue isosurfaces correspond to positive charge density deviation from the ground state, $\rho(r,t) - \rho(r,t=0) = 10^{-6}\text{Å}^{-3}$, and red isosurfaces to the corresponding negative deviation. In the transverse excitation (bottom), the isosurface values were 10^{-7}Å^{-3}. The two excitations were induced via longitudinal or transverse polarized enveloped laser pulses (See eq 4.10), with $w =$

$2\pi/\omega_0$ and $t_0 = 5w$; the values of the driving frequencies ω_0 are shown in Figure 4.4, along with the time taken for half an oscillation to occur.

Two distinct mechanisms of excitation are clearly visible in Figure 4.4. The longitudinally excited charge density (B_b state, top) sloshes back and forth along the π^* orbitals along the acene backbone; at the extrema, the charge density has piled up at one end of the molecule, with corresponding depletion (hole) on the opposite end. After transverse excitation (L_a state; bottom), however, the density is driven from delocalized π orbitals across the acene and forced to populate the orbitals above and below the $C - H$ bonds, which leads to alternating "fingers" of accumulated charge, and thus alternating $\cdots\ C^{\delta+}C^{\delta-}C^{\delta+}C^{\delta-}\ \cdots$ atoms along the acene. In a valence bond picture this is an ionic-like excitation, in agreement with previous analyses.[18, 20] The intra-molecular charge-transfer-like character (or charge transfer in disguise) is not due to long-range pile up of charge but instead arises from this ionic-like character. Here, range-separated functionals perform well because they are able to capture interaction between these regions of alternating charge and hole. This is related to Kuritz et al.'s discussion, where a state is characterized as charge-transfer-like based on minimal overlap of auxiliary orbitals.[19]

RT-TDDFT can also shed light on the origin of the red-shifts. As the acenes increase in length, the time taken to oscillate increases (frequency decreases) for both the transverse and longitudinal excitations. Although not immediately obvious, the red-shifts of both excitations can be rationalized in a similar way. The simplest

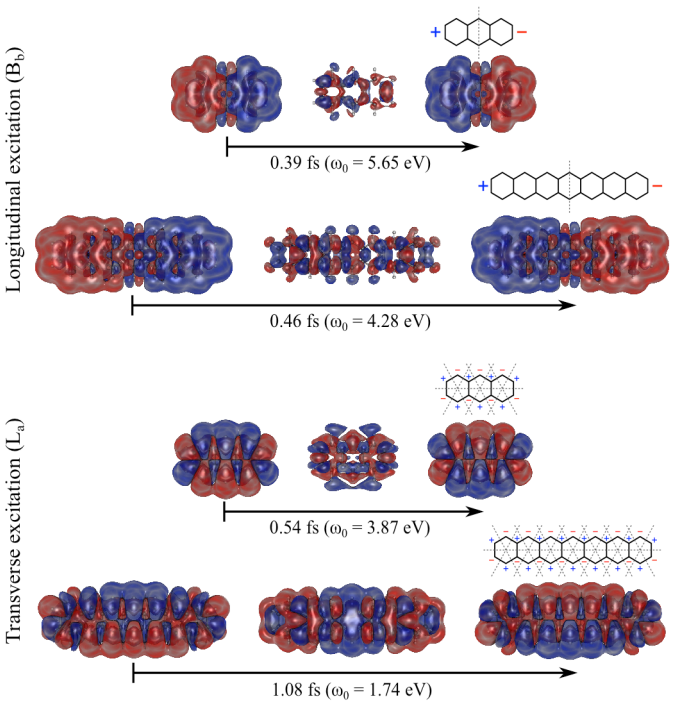

Figure 4.4 Real-time TDDFT (6-31G**/BNL) isosurface snapshots of the deviation of the charge density from the ground state for anthracene (N=3) and heptacene (N=7), after resonant excitation (frequencies shown in eV). Positive deviation (more charge density than in the ground state) is shown in blue, while negative deviation (less charge density than ground state) is shown in red.

physical description for this comes from the perimeter free electron orbital (PFEO) theory,[1,58] which models the π electrons as being confined in an oval-shaped infinite potential with no other electron-nuclear or electron-electron interactions. This leads to a particle-on-a-ring wavefunction for each π electron; a particular electronic state is then characterized by the total ring quantum number Q, which is the sum of the individual ring quantum numbers. The number of nodal planes for a particular state is then Q, with alternating positive and negative charge build-up at each antinode. This is clearly visible in Figure 4.4, where the charge density deviations at the maxima of the oscillations (i.e., the excited electronic states) directly match up to the PFEO predictions. In anthracene, for example, the excited state charge density of the B_b state corresponds to a $Q = 1$ state (one node; high longitudinal dipole moment), whereas the L_a state corresponds to $Q = 7$ (seven nodes; low but non-zero transverse dipole moment). The transition to $Q = 7$ (L_a) requires less energy than to $Q = 1$ (B_b), which is a consequence of Hund's rule.[1] Larger acenes have larger circumferences, and are thus their excitation energies are red-shifted.

4.4 Conclusions

In summary, we have computed the L_a and L_b vertical excitation energies for the acenes ranging from anthracene to heptacene, using a broad spectrum of excited-state theoretical approaches. High accuracy coupled cluster calculations (CR-EOMCCST(T)) agree extremely with experiment well for both states, and thus serve as a baseline for validating the lower level theories. Global hybrid TDDFT (e.g, B3LYP) perform poorly for the L_a state as expected, whereas range-separated hybrid (RSH) TDDFT (e.g, CAM-B3LYP, LC-BLYP, etc) better describe the ionic L_a state, at a cost of lost accuracy for the L_b state. Real-time RSH TDDFT visualization shows that the excited state charge densities are consistent with the predictions of perimeter free electron orbital (PFEO) theory, and the red-shift of the excitations are due to particle-on-a-ring-like confinements. For the semi-empirical methods, with proper parametrization ZINDO rivals range-separated hybrids in accuracy, at a fraction of the computational cost. This suggests a multi-tiered approach to modeling complicated acene derivatives, as well films and crystals of these molecules: high accuracy coupled cluster calculations validate RSH TDDFT calculations on small (perhaps pairs) of molecules, which in turn enables careful parametrization of semi-empirical calculations capable of modeling large systems.

References

(1) Pope, M.; Swenberg, C. E. Electronic processes in organic crystals and polymers, 2nd ed.; Oxford University Press: Oxford, U.K., 1999; Chapter 1, pp 7_12.

(2) Picciolo, L. C.; Murata, H.; Kafafi, Z. H. Appl. Phys. Lett. 2001, 78, 2378.

(3) Wolak,M.A.;Jang,B.B.;Palilis,L.C.;Kafafi,Z.H.J.Phys.Chem. B 2004, 108, 5492–5499.

(4) Xu,Q.;Duong,H.M.;Wudl,F.;Yang,Y.Appl.Phys.Lett.2004, 85, 3357.

(5) Lin,C.Y.;Wang,Y.C.;Hsu,S.J.;Lo,C.F.;Diau,E.W.G.J.Phys. Chem. C 2009, 114, 687–693.

(6) Lloyd, M. T.; Mayer, A. C.; Subramanian, S.; Mourey, D. A.; Herman, D. J.; Bapat, A. V.; Anthony, J. E.; Malliaras, G. G. J. Am. Chem. Soc. 2007, 129, 9144–9149.

(7) Jiang, Y.; Okamoto, T.; Becerril, H. A.; Hong, S.; Tang, M. L.; Mayer, A. C.; Parmer, J. E.; McGehee, M. D.; Bao, Z. Macromolecules 2010, 42, 6361_6367.

(8) Sheraw,C.D.;Zhou,L.;Huang,J.R.;Gundlach,D.J.;Jackson, T. N.; Kane, M. G.; Hill, I. G.; Hammond, M. S.; Campi, J.; Greening, B. K.; Francl, J.; West, J. Appl. Phys. Lett. 2002, 80, 1088–1090.

(9) Merlo, J. A.; Newman, C. R.; Gerlach, C. P.; Kelley, T. W.; Muyres, D. V.; Fritz, S. E.; Toney, M. F.; Frisbie, C. D. J. Am. Chem. Soc. 2005, 127, 3997–4009.

(10) Tang, M. L.; Reichardt, A. D.; Miyaki, N.; Stoltenberg, R. M.; Bao, Z. J. Am. Chem. Soc. 2008, 130, 6064–6065.

(11) Lin,Y.Y.;Gundlach,D.J.;Nelson,S.F.;Jackson,T.N.Electron Device Lett., IEEE 1997, 18, 606–608.

(12) Klauk,H.;Halik,M.;Zschieschang,U.;Schmid,G.;Radlik,W.; Weber, W. J. Appl. Phys. 2002, 92, 5259.

(13) Kim,G.H.;Shtein,M.;Pipe,K.P.Appl.Phys.Lett.2011,98,093303.

(14) Anthony,J.E.Chem.Rev.2006,106,5028–5048.

(15) Anthony,J.E.Angew.Chem.,Int.Ed.2008,47,452–483.

(16) Kawashima, Y.; Hashimoto, T.; Nakano, H.; Hirao, K. Theor. Chem. Acc. 1999, 102, 49–64.

(17) Wong, B. M.; Hsieh, T. H. J. Chem. Theory Comput. 2010, 6, 3704–3712.

(18) Richard,R.M.;Herbert,J.M.J.Chem.TheoryComput.2011,7, 1296–1306.

(19) Kuritz, N.; Stein, T.; Baer, R.; Kronik, L. J. Chem. Theory Comput. 2011, 7, 2408–2415.

(20) Grimme, S.; Parac, M. ChemPhysChem 2003, 4, 292–295.

(21) Bak, K. L.; Koch, H.; Oddershede, J.; Christiansen, O.; Sauer, S. P. A. J. Chem. Phys. 2000, 112, 4173–4185.

(22) Peach,M.J.G.;Benfield,P.;Helgaker,T.;Tozer,D.J.J.Chem. Phys. 2008, 128, 044118.

(23) Huang,L.;Rocca,D.;Baroni,S.;Gubbins,K.E.;Nardelli,M.B. J. Chem. Phys. 2009, 130, 194701.

(24) Runge,E.;Gross,E.K.U.Phys.Rev.Lett.1984,52,997.

(25) Petersilka,M.;Gossmann,U.J.;Gross,E.K.U.Phys.Rev.Lett. 1996, 76, 1212–1215.

(26) Casida,M.E.InRecentAdvancesinDensityFunctionalMethods; Chong, D. P., Ed.; World Scientific Publishing: River Edge, NJ, 1995; Vol. 1, Chapter 5, pp 155_192.

(27) Valiev, M.; Bylaska, E. J.; Govind, N.; Kowalski, K.; Straatsma, T. P.; Van Dam, H. J. J.; Wang, D.; Nieplocha, J.; Apra, E.; Windus, T. L.; de Jong, W. A. Comput. Phys. Commun. 2010, 181, 1477–1489.

(28) Stewart,J.J.P.J.Comput.Chem.1989,10,209–220.

(29) MOPAC 6.0. http://ccl.net/cca/software/MS-WIN95-NT/ mopac6/index.shtml (accessed September 2011).

(30) Bartell, L. A.; Wall, M. R.; Neuhauser, D. J. Chem. Phys. 2010, 132, 234106.

(31) Zerner, M. C. et al. ZINDO-MN, version 2011; Quantum Theory Project, University of Florida: Gainesville, FL; Department of Chemistry, University of Minnesota: Minneapolis, MN, 2011.

(32) Hirata, S.; Head-Gordon, M. Chem. Phys. Lett. 1999, 302, 375–382.

(33) Bartlett,R.J.;Musiaz,M.Rev.Mod.Phys.2007,79,291–352.

(34) Kowalski, K.; Krishnamoorthy, S.; Villa, O.; Hammond, J. R.; Govind, N. J. Chem. Phys. 2010, 132, 154103.

(35) Watts, J. D.; Bartlett, R. J. Chem. Phys. Lett. 1995, 233, 81–87.

(36) Watts,J.D.;Bartlett,R.J.Chem.Phys.Lett.1996,258,581–588.

(37) Christiansen, O.; Koch, H.; Jørgensen, P. J. Chem. Phys. 1996, 105, 1451.

(38) Hirata, S.; Nooijen, M.; Grabowski, I.; Bartlett, R. J. J. Chem. Phys. 2001, 114, 3919.

(39) Shiozaki, T.; Hirao, K.; Hirata, S. J. Chem. Phys. 2007, 126, 244106.

(40) Manohar,P.U.;Krylov,A.I.J.Chem.Phys.2008,129,194105.

(41) Kowalski,K.;Piecuch,P.J.Chem.Phys.2004,120,1715.

(42) Kowalski,K.;Piecuch,P.J.Chem.Phys.2001,115,2966.

(43) Wzoch,M.;Lodriguito,M.D.;Piecuch,P.;Gour,J.R.Mol.Phys. 2006, 104, 2991.

(44) Piecuch,P.;Gour,J.R.;Wzoch,M.Int.J.QuantumChem.2009, 109, 3268–3304.

(45) Kowalski,K.J.Chem.Phys.2009,130,194110.

(46) Raghavachari,K.;Trucks,G.W.;Pople,J.A.;Head-Gordon,M. Chem. Phys. Lett. 1989, 157, 479–483.

(47) Lopata, K.; Govind, N. J. Chem. Theory Comput. 2011, 7, 1344–1355.

(48) Anderson,W.P.;Cundari,T.R.;Zerner,M.C.Int.J.Quantum Chem. 1991, 39, 31–45.

(49) Stephens, P. J.; Devlin, F. J.; Chabalowski, C. F.; Frisch, M. J. J. Phys. Chem. 1994, 98, 11623–11627. (50) Yanai, T.; Tew, D. P.; Handy, N. C. Chem. Phys. Lett. 2004, 393, 51–57.

(51) Rohrdanz,M.A.;Martins,K.M.;Herbert,J.M.J.Chem.Phys. 2009, 130, 054112.

(52) Baer,R.;Neuhauser,D.Phys.Rev.Lett.2005,94,043002.

(53) Lambert,W.R.;Felker,P.M.;Syage,J.A.;Zewail,A.H.J.Chem. Phys. 1984, 81, 2195.

(54) Hirao,K.Chem.Phys.Lett.1992,190,374–380.

(55) Hirao,K.Chem.Phys.Lett.1992,196,397–403.

(56) Christiansen, O.; Koch, H.; Jørgensen, P. Chem. Phys. Lett. 1995, 243, 409–418.

(57) Baer,R.;Livshits,E.;Salzner,U.Annu.Rev.Phys.Chem.2010, 61, 85–109.

(58) Platt,J.R.J.Chem.Phys.1949,17,484–495.

(59) Blender;TheBlenderFoundation:Amsterdam,TheNetherlands, 2010.